FINAL PUBLISHABLE JRP REPORT

JRP-Contract number	IND08
JRP short name	MetMags
JRP full title	Metrology for advanced industrial magnetics
Version numbers of latest contracted Annex Ia and Annex Ib against which the assessment will be made	Annex Ia: V1.0 Annex Ib: V1.0
Period covered (dates)	From 01 July 2011 to 30 June 2014
JRP-Coordinator:	
Name, title, organisation	Hans Werner Schumacher, Dr, PTB
Tel:	+49 531 592 2500
Email:	Hans.w.schumacher@ptb.de
JRP website address	http://www.ptb.de/emrp/metmags.html
Other JRP-Partners	
Short name, country	CMI, Czech Republic INRIM, Italy NPL, United Kingdom TUBITAK, Turkey

REG1-Researcher (associated Home Organisation)	James Haigh HEL, United Kingdom	Start date: 01 July 2011 Duration: 36 months
REG2-Researcher (associated Home Organisation)	Günter Reiss UBI, Germany	Start date: 01 September 2012 Duration: 22 months
ESRMG1-Researcher (associated Home Organisation)	Ales Zikmund CMI, Czech Republic	Start date: 01 September 2012 Duration: 06 months

Report Status: PU Public

European Metrology Research Programme
Programme of EURAMET

The EMRP is jointly funded by the EMRP participating countries within EURAMET and the European Union

TABLE OF CONTENTS

1 Executive Summary 3
2 Project context, rationale and objectives 4
3 Research results 5
4 Actual and potential impact 27
5 Website address and contact details 30
6 List of publications 31

1 Executive Summary

Introduction

This project has delivered underpinning metrology to foster the development, testing and calibration of advanced magnetic sensors by the European magnetic sensor industry.

The Problem

The automotive branch is one of the most important European industrial sectors and is one of the driving forces for advanced magnetic sensor development. Many sensors are used in today's cars e.g. for motor control or for passenger safety applications via systems such as antilock braking systems (ABS) and electronic stability program (ESP), and many more will be required in the future. At the same time these sensors will be required to meet ever tighter specifications that need to be verified by suitable metrology.

In addition to the automotive industry, there are many other industrial applications of magnetic sensors in fields such as geological exploration, aerospace, biomedical, consumer products, information and communications technology (ITC). In all these fields improved sensor devices need to be developed by the European industry and they need to be able to meet tighter specifications, with respect to reliability, operation temperature, device size, field range and calibration uncertainty, etc. Hence, the European sensor industry requires underpinning metrology to develop, produce, test, and calibrate advanced industrial magnetic sensor devices to stay competitive in the global market.

The Solution

To address these needs of the European magnetic sensor industry the MetMags project has delivered:

1. Metrological tools and methods for industrial magnetic sensor development,
2. Metrological in-line tools and methods for sensor production, and
3. Metrology for sensor testing and calibration.

Impact

All these new calibration facilities and metrology tools and methods will enable the European magnetic sensor industry to develop, produce and calibrate more reliable magnetic sensors to stay competitive in the global market. The project results have been efficiently disseminated to stakeholders via various paths and during the project the research outputs have already been used by industry generating significant early impacts.

Examples for early impact include:

- New metrology tools have enabled a world leading European based magnetic sensor producer to identify device defects generated by a specific processing step. The manufacturing process was subsequently optimised allowing the subsequent high volume production of highly reliable magnetic anisotropic magneto resistance (AMR) sensors.
- New low field calibration facilities were used to measure the magnetic moment of components for the ESA EarthCARE mission. These kind of magnetic cleanliness measurements significantly contribute to the success of present and future European space missions.
- Reliable magnetic field measurements are underpinned by a *Best Practice Guide for Magnetic Field Measurements* which is available online. This can be seen as a first step towards standardisation with impact on magnetic field measurements in industry, bio-medical, safety and health.

The novel European metrology infrastructure will enable European sensor manufacturers to meet tighter specifications of the application sectors. In the long term it will strengthen one of the key enabling European industries with strong economic and social impacts for Europe.

2 Project context, rationale and objectives

Magnetic sensors can be found in a broad range of products in various industrial fields like consumer electronics, ICT, and the automotive industry. The fast product development in these fields creates the need for advanced magnetic sensors, which have significantly improved specifications with respect to for example resolution, reliability, size, signal-to-noise ratio, and operation temperature, among others. To verify the sensor specifications and to enable advanced sensor development requires an underpinning metrology for their testing, characterisation, and calibration.

The automotive branch is one of the most important European industrial sectors. At the same time it is one of the driving forces for advanced magnetic sensor development: Many magnetic sensors are used in today's cars e.g. for motor control to optimised fuel consumption or for passenger safety applications like ABS and ESC. Automotive magnetic sensor systems thus significantly contribute to the European goals for the reduction of greenhouse gases as well as to European traffic safety. Note that EC regulation No 661/2009 requires ESC systems on all vehicles from Nov. 1st 2014. It is obvious that such safety relevant sensors have to meet the highest specifications with respect to device reliability. Many more magnetic sensor devices will be required in the future cars. At the same time these sensor will also be required to meet tighter and tighter specifications which need to be verified by suitable metrology tools.

In addition to automotive many other industrial applications of magnetic sensors can be found e.g. in geological exploration, aerospace, biomedical, consumer products, ITC, and others. In all these fields improved sensor devices need to be developed by the European industry, again with advanced specifications, with respect to various aspects like reliability, operation temperature, device size, field range, and calibration uncertainty, among others. To underpin these advanced developments the European sensor industry requires metrology to develop, produce, test, and calibrate advanced industrial magnetic sensor devices to be able to compete in the global market.

Therefore the goal of the project was to foster development, production and calibration of advanced magnetic sensors by the European sensor industry and to advance their application in present and emerging technologies. This goal was achieved by providing the metrological framework for the **development**, **production**, and **testing and calibration** of advanced magnetic sensors.

The three key objectives of the project were to:

Objective 1: Develop metrological tools and methods for industrial magnetic sensor development (traceable characterisation of advanced materials, optimisation of sensor devices, emerging new concepts)

Objective 2: Develop metrological in-line tools and methods for sensor production (traceable measurement of magnetic parameters of devices such as thin films, multilayer stacks, patterned magnetic microstructures, individual magnetic microdevices etc.)

Objective 3: Develop metrology for sensor testing and calibration (metrological chain including specific coil setups, reference and test magnetic materials, metrological tools for testing magnetic properties in HF range (GHz), stress and reliability properties).

Project Organisation

To efficiently meet the three objectives the project was organised in the following five technical work packages (WPs). A brief overview of the WP structure with participants, key tasks and interactions between the WPs is given. More details on the work of the technical WPs is provided in the next section of this report.

- <u>WP1: Metrology for AMR thin film sensors (INRIM, PTB, TUBITAK UME)</u>
  This WP developed metrological tools and methods to relate performance of future ultra-small AMR sensors to the occurrence of local defects, geometrical properties and stress. It was supported by WP4. The results obtained on domain wall (DW)-pinning at defects are relevant for WP5 (DW-devices).
- <u>WP2: Magnetic Sensors Testing and Calibration (NPL, CMI, PTB)</u>
  This WP expanded the parameter range of traceable calibration of advanced magnetic sensors. Specific tasks were calibration at operational temperature (cp. WP4), noise measurements, and three axial calibrations. Calibration facilities developed in WP2 were used to investigate sensors from all other WPs. A best practice guide for field measurements was developed and disseminated to the stakeholders.

- WP3: Metrology for spin torque materials and devices (PTB, INRIM)
  This WP provided metrological tools for characterisation and in line testing of spin torque sensor materials and devices. One deliverable was non-destructive metrology of key spin torque material parameters. It was supported by modelling of WP4 and supports DW-dynamics measurements of WP5.
- WP4: Micromagnetic numerical modelling (INRIM, PTB)
  This WP provided procedures to validate micromagnetic simulation tools used for industrial sensor development. Validated models resulting from this cross cutting WP were applicable to all technical WPs. Specific tasks addressed modelling of thermal effects (WP2), modelling of AMR sensors (WP1) and modelling of DW-sensors (WP5).
- WP5: Metrology for advanced magnetic sensor concepts (NPL, INRIM, PTB)
  This WP provided metrology for advanced micro Hall sensors and for the emerging concept of domain wall sensors. This WP heavily interacted with simulations within WP4.

3 Research results

Overview of the research results

The project has delivered metrology tools and methods that will enable the European high-technology industry to progress in some of its most progressive branches and to strengthen the European position in global competition. The project results relate to the three scientific and technical objectives in the following way:

Objective 1: *Develop metrological tools and methods for industrial magnetic sensor development.*

- Validated modelling tools for the micromagnetic modelling of micro- and nano-scale magnetic thin film sensors have been developed. They allow reliable modelling of the most important magnetic sensor device properties including magnetic domain structure, magnetisation reversal curves, magneto transport properties and sensitivity. Such reliable modelling is a key towards efficient model based future sensor development (WP4).
- A metrology system for the characterisation of novel magnetic domain wall sensor devices has been established. The systems allows for accurate and complete mapping of the domain wall-related change in the anisotropic magnetoresistance as a function of the magnitude and orientation of the applied magnetic field. It allows identifying highly reproducible transitions between domain states and hence to determine the optimal working parameters to underpin the development of specific novel domain wall sensor devices (WP5).
- A new micro Hall sensor based method for the calibration of the magnetic stray fields of magnetic near field probes for MFM has been developed. It will in the future allow MFM base traceable measurements of magnetic stray field on the nano scale with strong implications device testing and materials research.
- Metrology tools based on magneto transport and magnetic imaging under variable fields and strain conditions for optimisation and development of future AMR sensors (WP1).
- Inductive metrology for key material parameters of magnetic multilayer stacks such as the damping, the anisotropies, and the critical current density j_C of spin torque sensor materials (WP3).

Objective 2: *Develop metrological in-line tools and methods for sensor production.*

- A method for the fast and non-destructive inductive determination of key material parameters for Spin-Torque (ST) materials has been developed and tested. It allows for the first time to determine the key material parameter of the ST critical current density in a lithography-free process. This method will allow both more efficient ST material development as well as fast in line process control (WP3)
- Magnetic force microscopy in variable magnetic fields and under variable applied stress has been established. It allows imaging details of the magnetisation reversal process to test and verify the predicted magnetisation reversal in magnetic sensor devices and prototypes. It further allows testing the influence of strain on the magnetisation processes. This allows evaluating the robustness of sensor devices for industrial applications in harsh environments (WP1).

Objective 3: *Develop metrology for sensor testing and calibration.*

- A novel calibration procedure for the calibration of tri-axial Helmholtz coil systems was developed. The novel method is simple, versatile and reliable. It allows reliable on-site calibrations of industrial or academic tri-axial coil setups with low calibration uncertainty. As opposed to other calibration approaches the calibration does require complex on earth's field compensation equipment. The calibration principle was verified at CMI's suburban calibrating facility with 5nT p-p noise. An expanded uncertainty of 0.05 degrees was achieved for calibration of the orthogonality. The sensitivity was calibrated with a low extended uncertainty of less than 450 ppm (WP2).
- A portable three-axis SQUID system for the determination of the magnetic noise vector field behaviour of industrial facilities that produce a nominally zero magnetic environment. Explicitly for metrological applications, SQUID magnetometers with precise calculable SQUID loops have been designed, fabricated and characterised showing ultra-high field sensitivity of typically of 7.006 nT/Φ_0 ± 0.3 %. These systems are now available for the on-site noise metrology magnetic shielding (WP2).
- A low magnetic field facility was equipped with a magnetic shielding and thermal isolation, to produce a magnetically and thermally stable environment for noise measurements down to a frequency of 0.1 mHz. Additionally the system was equipped with temperature forcing system now enabling precision calibrations of sensitive magnetometers operational temperatures in the range of -55 °C to 125 °C (WP2).
- A best practise guide for magnetic field measurements (WP2)
- Tools for strain reliability testing of AMR sensors (WP2).
- Metrology and simulation tools for inductive testing of magnetic properties in the GHz range (WP3).

In the following a detailed description of the technical work and results of the five technical work packages will be given.

WP1: Metrology for AMR sensors

AMR sensors are highly important for many industrial applications like position and motion sensors, electronic compasses and automotive safety systems like anti blocking breaks (ABS) and electronic stability systems (ESC). To meet the high reliability standards and low failure rate needed for safety relevant devices requires underpinning metrology for AMR sensor testing.

This WP has provided:

- Magnetic force microscopy tools suitable for magnetic domain imaging in variable magnetic fields and under variable applied stress for the characterization of industrial AMR sensors.
- Metrology tools based on magneto transport and magnetic imaging under variable fields and strain conditions for optimisation and development of future AMR sensors.
- Studies of the magneto transport and magnetization reversal behaviour of advanced AMR sensor prototypes.

Magnetic imaging of AMR sensors

Magnetic force microscopy allows for a high resolution local characterisation of the magnetic microstructure of patterned sensor materials. In this project a microscopic characterisation of the sensor magnetisation response on magnetic in plane fields was requested by the stakeholders. Therefore, PTB designed and manufactured a sample stage for a commercial MFM scanning head that allows the reliable application of magnetic fields along any in-plane direction during the MFM imaging process (two permanent magnets are precisely positioned by stepper motors and the sample can be rotated).The field values are measured at the position of the sample. The stage was completed and tested. Fields from 0 to 167 mT can be applied.

This setup was used to perform detailed MFM investigations on a large number of patterned elements of different sensors provided by the collaborator. These investigations point out the presence of complex domain structures revealing closure and vortex domains in several parts of the sample. The measurement of an unexpected intrinsic anisotropy of the magnetic thin films was a key finding. Furthermore it could be shown, that imperfections in the material have a strong pinning effect on domain walls. Figure 1 exemplarily shows MFM images of domain patterns of sensor elements at different parts of the sensor area. The new metrology was used to evaluate the impact of a wafer processing step on the sensor performance and the underlying nanomagnetics processes. Several reports on the results were sent to the industrial collaborator. On the base of these results the sensor production process was reconsidered by the collaborator.

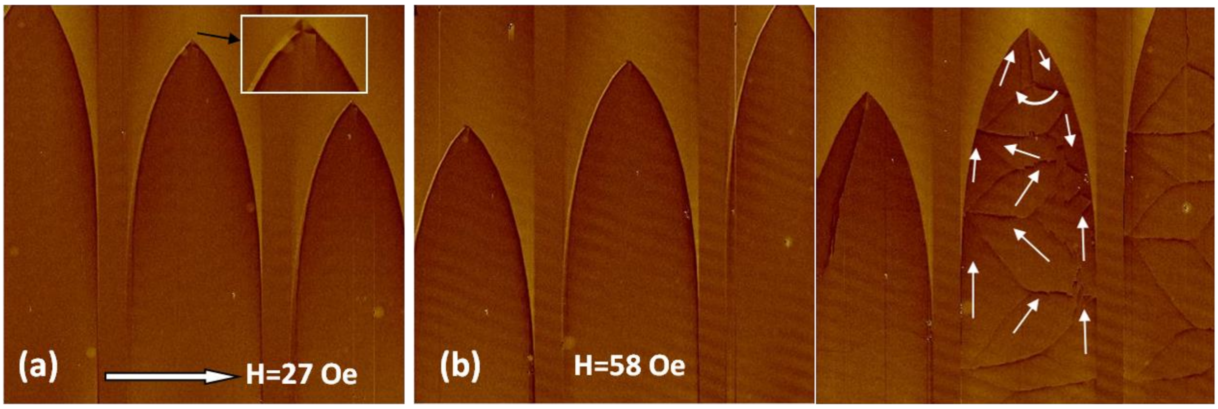

Figure 1: MFM images of patterned sensor elements at a magnetic field of 27 and 58 Oe, and in a remanent state after applying a magnetic field of 58 Oe.

The presence of a uniaxial anisotropy has been confirmed by MOKE measurements. This was particularly evident in the patterned elements with a circular shape (especially the biggest ones), which do not display any (in-plane) shape anisotropy. In fact, after saturation with a magnetic field applied along the 0° direction, its subsequent removal left the circular elements in a remanent state with magnetic domain walls aligned at a non-zero angle. This in-plane uniaxial anisotropy is rather strong, as it is able to overcome shape anisotropy in the ellipsoidal-shaped elements of the pattern. Figure 2 shows in the two frames almost the same portion of the sample magnetised with a saturating magnetic field (left) and at remanence (right). In the latter case, clearly visible transverse domains are marked by the clear-dark vertical bars appearing in the three shortest ellipsoidal elements. In longer ellipsoidal elements such features have not been observed.

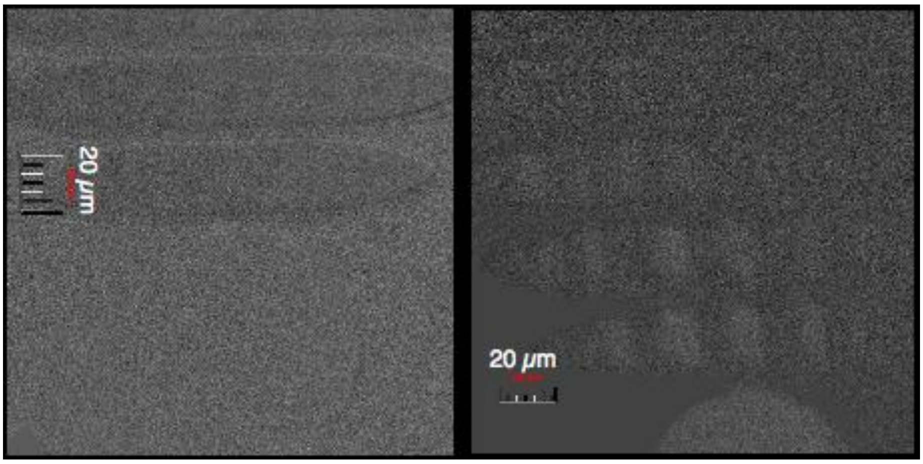

Figure 2: Left: saturating field along the horizontal direction. Right: magnetic remanence.

A consequence of this uniaxial anisotropy is that the shortest ellipsoidal elements were impossible to saturate even at the highest applied magnetic field (≈ 4000 A/m). In these elements, the reversal mechanism occurs through rotation of the magnetisation along the easy axis direction and fragmentation into multiple domains, followed by domain wall motion and last by rotation in the opposite direction when the applied magnetic field is sufficiently large. An example of magnetisation reversal process in these shortest ellipsoidal elements is shown in Figure 3, where from left to right and from top to bottom the different snapshots are taken at applied magnetic fields (along the horizontal direction) making a loop branch ($+H_{max} \rightarrow 0 \rightarrow -H_{max}$).

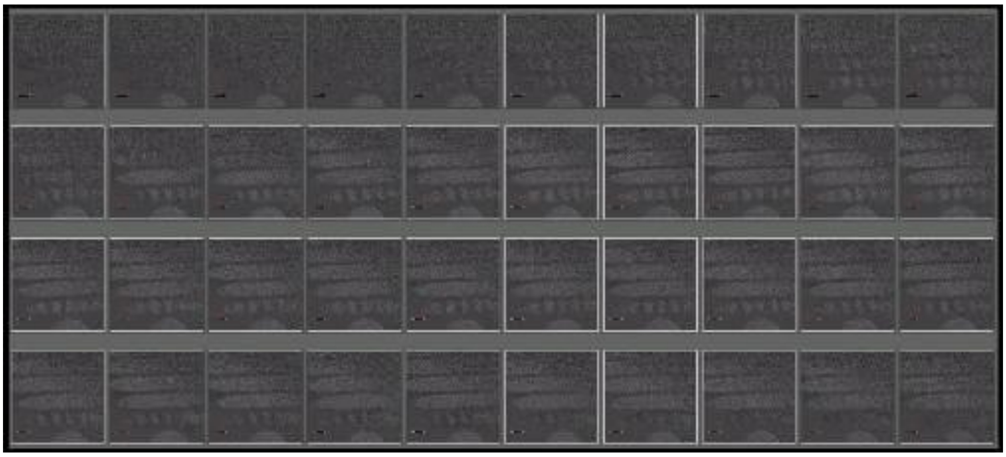

Figure 3: MOKE snapshots at different applied fields making a whole loop from left to right and top to bottom.

As a result, the hysteresis loops reported in Figure 4 display some expected and unexpected features. The ellipsoidal elements aligned along the 0° direction are characterised by more squared hysteresis loops, as expected, as the applied field lies along the shape anisotropy direction. However, irregularities are observed in the shortest elements (evidenced by the circle in the top-left frame of the figure), as the previously discussed uniaxial anisotropy is responsible for a different reversal mechanism and ultimately for reduced coercive field and remanence values. For the elements which are not aligned to the applied magnetic field, the coercive field is not significantly affected; however the loops shapes become less squared. The elements aligned at 90° with respect to the applied field are not saturated even at 4000 A/m, probably because of the demagnetising field due to the shape anisotropy.

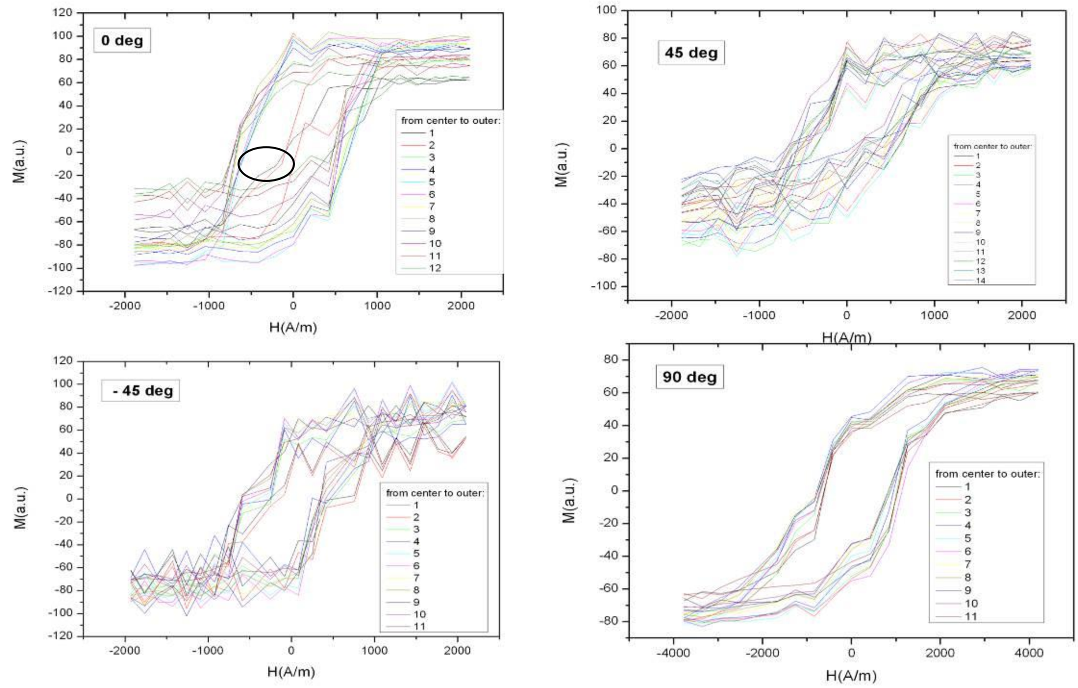

Figure 4: MOKE loops for elements having different orientations with respect to the applied field.

Magneto resistive metrology system for AMR sensors.

To relate the observed magnetic microstructure to the magnetoresisitive properties of the sensor, a local measurement of the magnetoresistance as a function of the applied in-plane field is required. Therefore, a resistive measurement system was provided that allows an electrical contacting of single individual elements in the patterned sensor material using “Picoporobe” wafer probes. An in-plane field up to 180 mT can be applied during the measurements. This allows to measure local AMR curves.

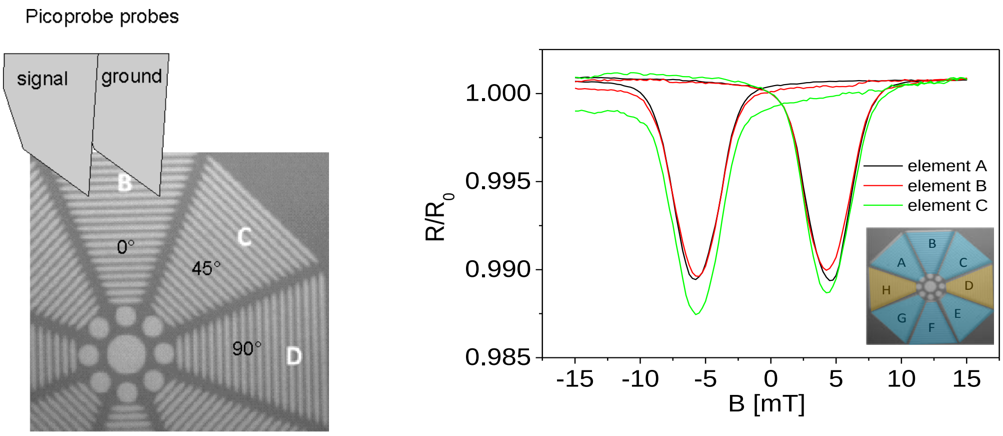

Figure 5: Schematic drawing of the local electric contacting scheme with wafer probes (right) and measurement results on AMR sensor elements with different orientations (field parallel to the stripes) (left).

Such characterisation can contribute to an understanding how local defects contribute to the sensor net signal via local variations of magnetisation and thus to the AMR.

Stress testing of AMR sensors

The aim of this task was to develop a stress tolerance testing procedure based on a device that allows for an application of well-defined flexural stress to thin films and components. Therefore, the in-plane field MFM stage was complemented by a specially developed unit that allows a controlled bending of the substrate thereby applying mechanical stress. This expansion of our MFM imaging facilities allows AMR sensor imaging in the presence of mechanical strain beyond 1 GPa *and* under applied in-plane field in field ranges from 0.6 mT -17.5 mT or 5.8 mT -166.8 mT, depending on the permanent magnets.

Figure 6 a shows the stress unit and the complete stage including the in-plane field unit. Stress unit and in-plane filed unit are driven by stepper motors and computer controlled. The tensional stress σ at the substrate surface can be calculate form the deflection of the substrate if the materials Young's Modulus and Poisson ratio are known.

In stress measurements on samples from our collaborator at σ=300 MPa showed weak influence on the domain pattern as expected for Permalloy with its low magnetostriction. In multi domain states in some cases a slight motion of domain walls after the bending was observed, however there is no clear evidence for a causal relationship to the stress. As consequence the tested commercial AMR sensor devices do not suffer from stress induced degradation of sensor properties.

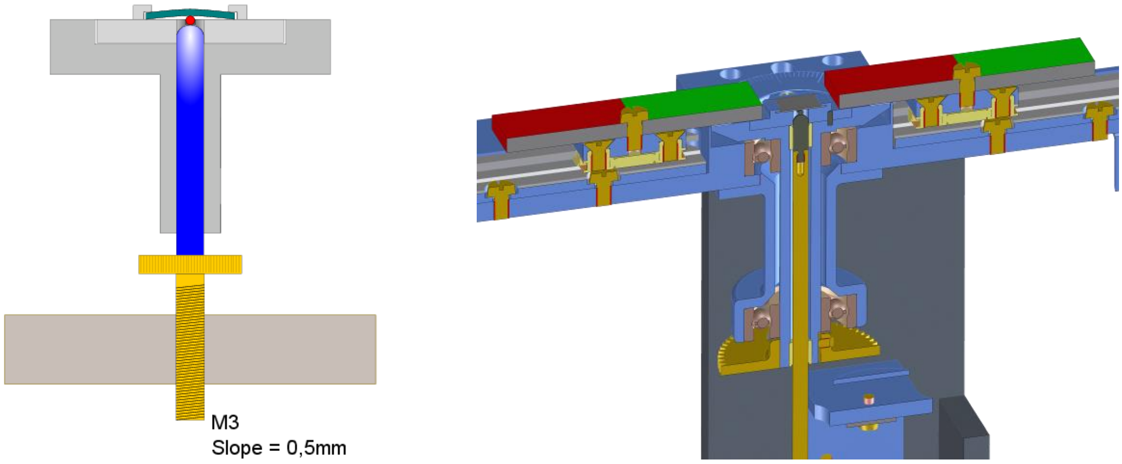

Figure 6: Specially developed stress unit (left) and complete MFM measurement stage including stress unit, sample rotation and in-plane field unit (right).

Laboratory investigations of fundamental AMR sensor elements

The aim of this task is to develop and characterise model systems for different defects that can serve as reference standards for AMR sensors characterisation techniques.

With MFM, films of soft magnetic materials with antidot arrays and well defined artificial defects were analysed. The incorporation of antidot arrays in AMR sensor materials allows an engineering of their magnetic properties, i.e. a direct adjustment of the sensor response. Therefore, here antidot arrays in Permalloy thin films are regarded as model systems.

Lattices of circular antidots in a 30 nm thick Permalloy film with *small* antidot diameters (*d*=60, 80, and 100 nm) and a *low* filling factor (~0.6) in Permalloy films were fabricated at PTB by e-beam lithography and lift-off process. The influence of antidot diameter, antidot spacing, and the aspect ratio of the lattice on the remanent domain configuration are investigated by magnetic force microscopy and supported by micromagnetic simulations. In such model AMR systems the influence of defects on the magnetic domain structure and on remagnetisation processes was characterised.

To support the results from section 1.1, the micromagnetics of sensor elements was simulated with a Landau-Lifshitz-Gilbert micromagnetic simulator. Figure 7 shows some simulation results of the magnetisation followed by calculated MFM images. The simulations are helpful to analyse and understand the experimental MFM images.

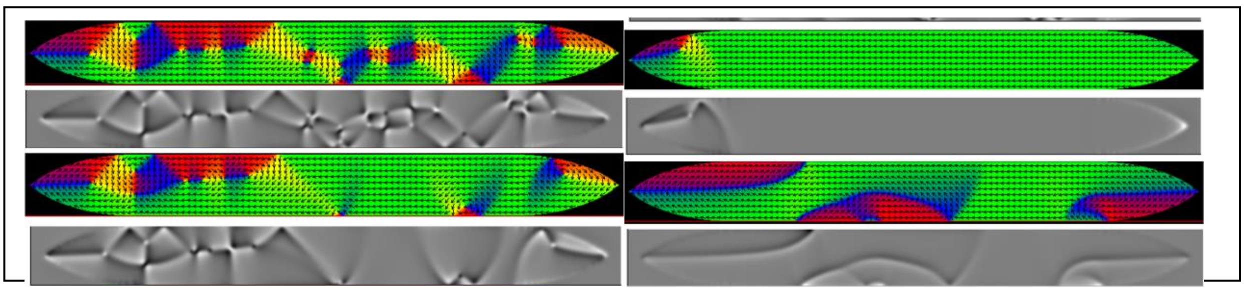

Figure 7: Simulated spin configuration in a sensor element during the relaxation of spins and corresponding calculated MFM images.

Arrays of antidots with larger diameter (280 and 480 nm) and in different lattice configurations (hexagonal and rhombic respectively) have also been prepared at INRIM by EBL on Permalloy thin films with a thickness of 30 nm. Typical arrays are shown in Figure 8.

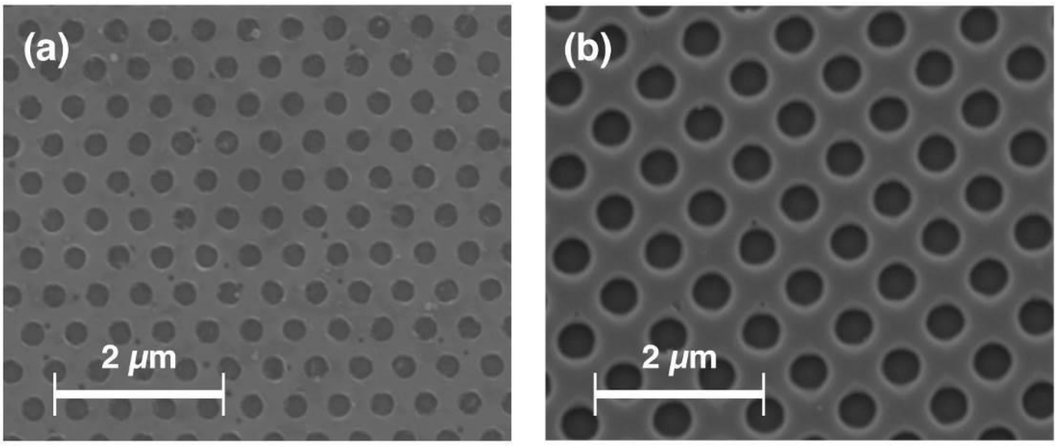

Figure 8: SEM images of $Ni_{80}Fe_{20}$ antidot arrays prepared by electron beam lithography having a hexagonal (a) and rhombic (b) lattice configuration.

Their magnetic and magneto-resistive properties have been investigated at room temperature through MFM and AMR measurements (see Figure 9). The effect of disorder has been then taken into account by a different approach, i.e. by preparing antidot arrays with hexagonal configuration with the technique of self-assembling of polystyrene nanospheres that intrinsically produces holes arrays with dislocations, grain boundaries and point defects. A typical antidot array prepared with this technique is shown in Figure 10, together with its typical AMR response. These data have been provided as input to WP4.

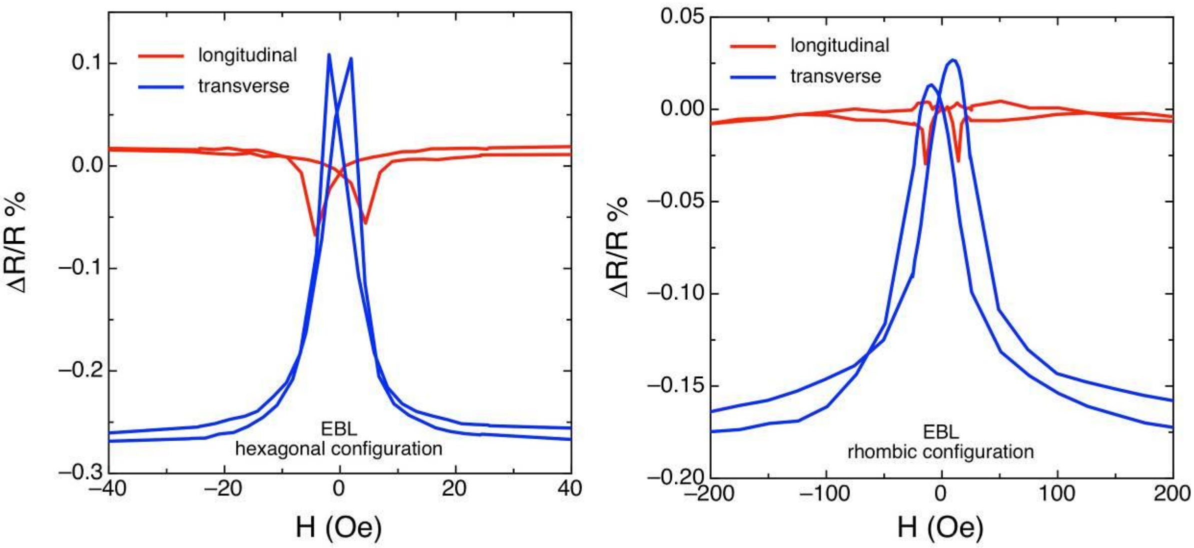

Figure 9: Room-temperature AMR measurements for hexagonal (left) and rhombic (right) antidot lattices prepared by EBL in the longitudinal (red curves) and transverse (blue curves) configurations.

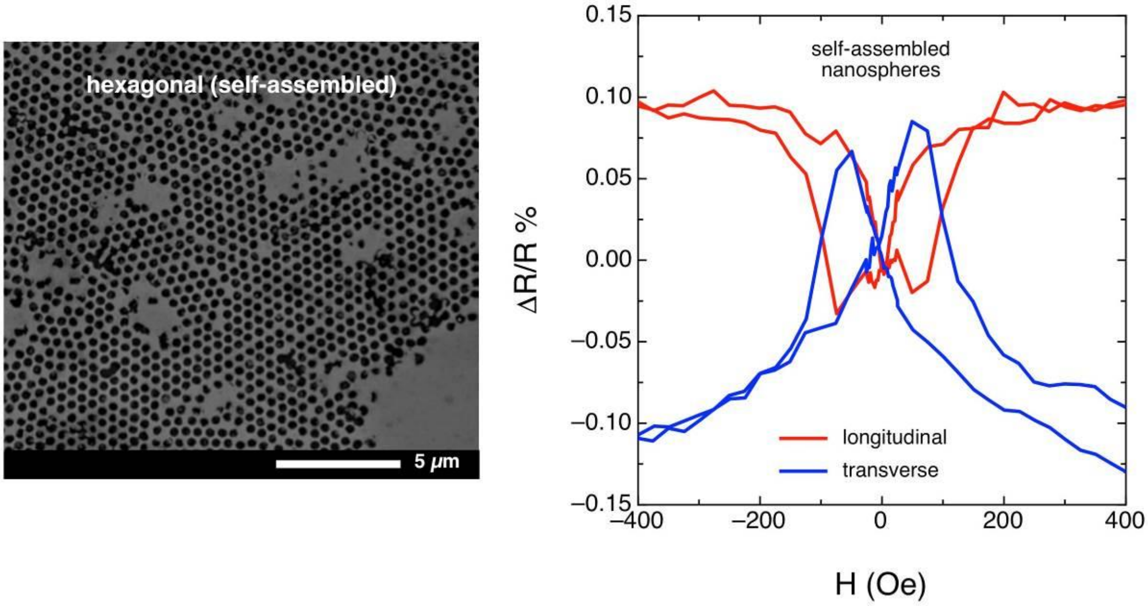

Figure 10: Left: SEM image of a $Ni_{80}Fe_{20}$ antidot array prepared by self-assembling of nanospheres. Right: corresponding room-temperature AMR measurements along the longitudinal (red curve) and transverse (blue curve) directions.

The detailed comparison of the experimental and simulated results in the different applied field configurations has provided an insightful description of the magnetisation reversal mechanisms and of their role in determining the field dependence of the AMR effect, together with lattice geometry. For ordered samples with both hexagonal and rhombic lattice, a consistently larger AMR signal in the transverse configuration has been detected and properly described by means of the micromagnetic model. Finally, the experimental analysis on less regular lattice samples (obtained via bottom-up technique) has put in evidence a larger coercivity and an isotropic behaviour.

WP2: Magnetic Sensors Testing and Calibration

Industrial stakeholders develop magnetic sensors with highest specifications for example with respect to noise or variable temperature environment. To traceably calibrate these advanced sensors high level calibration facilities are needed at the NMIs. These have been provided within WP2.

The combined effort of the partners involved in this Work Package has produced the following industry focused outputs:

- The Best Practice Guide “Generation and measurement of DC magnetic fields in the magnetic field range of 1 nT to 1 mT.”. The content of this guide was determined at an industry event held at NPL. A stakeholder said “Thank you for including what we thought was important (temperature, and non-perfect environment)”. The guide has been sent to stakeholders and other industries who requested a copy after the work was presented at EMSA 2014.
- A portable SQUID array for the determination of the noise behaviour of industrial facilities that produce a zero magnetic environment.
- Unique facilities for characterising sensitive magnetometers at temperatures in the range of -55 °C to 125 °C. This temperature range was decided at an industrial stakeholder event held at NPL. This exceeded the deliverable requirement of -40 °C to 100 °C.
- Angular calibration of sensor alignment for magnetometers with an extended uncertainty of 0.05°
- Capability for measuring noise at 0.1 mHz for use in International space projects.

Magnetic noise measurements at 0.1 mHz

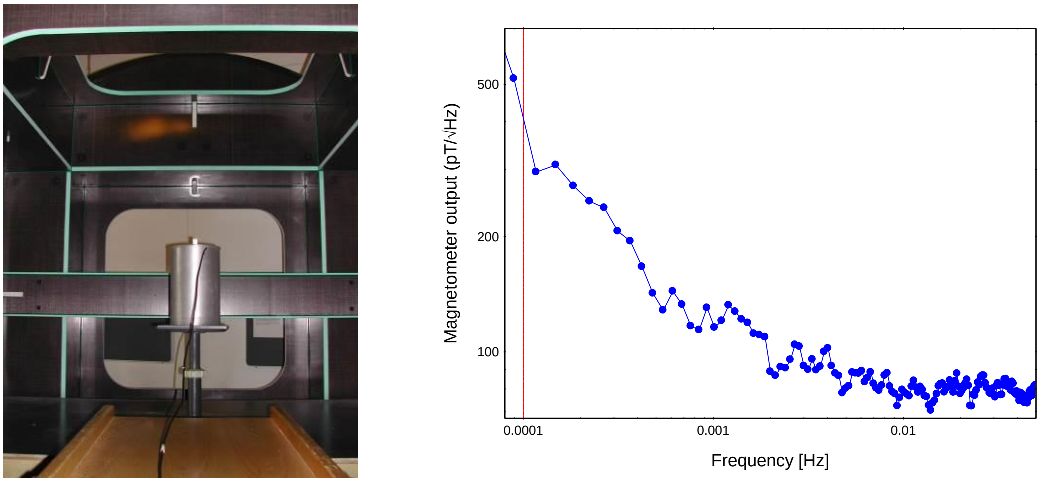

Figure 11: Left: Picture of low magnetic field facility at NPL including thermally isolated can. Right: magnetic noise of low magnetic field environment.

By incorporating a three layer can inside the NPL low magnetic field facility and thermally isolating the can, it was possible to produce a magnetically and thermally stable environment for noise measurements down to a frequency as low as 0.1 mHz.

This facility has been used by the European Space AGENCY (ESA) to produce a low noise gradiometer for magnetic cleanliness work. This gradiometer can be used for all future ESA missions that require magnetometers to deliver their science programme.

Facility for characterising magnetometers in the temperature range -55 °C to 125 °C

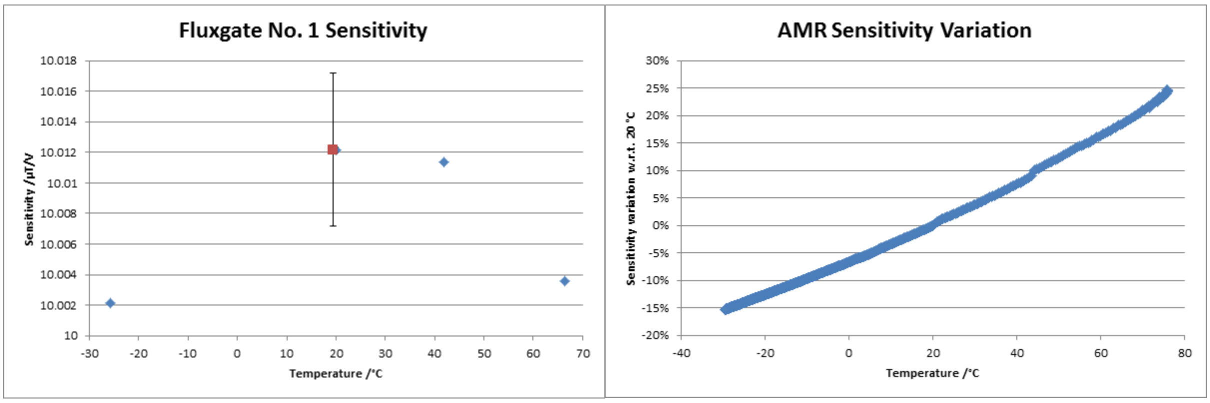

Figure 12: Examples for industrial calibration of sensors in the new facility of NPL. Left: fluxgate calibration (Bartington Inst. Ltd.), Right: AMR sensor calibration (NXP).

By incorporating a commercial forced air temperature system into the NPL low magnetic field facility in such a way that the AC magnetic cleanliness was not disturbed, a step change in the ability to characterise sensors for the automotive industry, geological exploration and space applications where the actual temperature experienced during their operation is significantly different to that used during their development and calibration has been achieved.

This facility has been used by Bartington Instruments Limited and NXP to determine the temperature coefficients for their fluxgate and AMR sensors respectively and the results are shown in Figure 12.

A portable SQUID array for the determination of the noise behaviour of industrial facilities

Explicitly for metrological applications, SQUID magnetometers, with precise calculable SQUID, were designed, fabricated and characterised The field sensitivity V_Φ has been determined with FEM calculations and measurements for comparison. A typical value of 7.006 nT/Φ_0 ± 0.3 % (k = 2) was found.

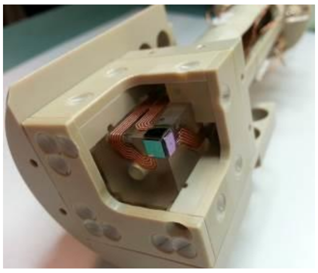

Figure 13: Sensor module with 6 SQUIDS.

Six of these SQUID magnetometers were selected to build a three-axis SQUID system (the number of sensors and the arrangement in two triples has been chosen for the purpose of enabling the calculation of the gradients in each axis from magnetometer measurements) (Figure 13).

The SQUIDs have been mounted directly to a Sapphire-cube and connected by a new type of wiring. In order to avoid mechanical vibrations, the SQUID module has been embedded in a mechanically solid cage. All parts are cooled in a Helium bath cryostat which h enables measurements to be made without refill in a period of at least two days.

Figure 14: SQUID system

For the reciprocal of the mutual inductance $1/M_f$ a typical value of 16.874 µA/Φ_0 was found for the six implemented devices, whereas the uncertainty of the measurement is ± 0.704 % (k = 2). The system noise, measured several times in the Berlin Magnetically Shielded Room (BMSR), is definitely below the requested 10 fT/Hz$^{1/2}$ in the white noise frequency range.

The SQUID system (Figure 14) has been used to measure the noise induced by a shielding layer of project partner CMI and to estimate the shielding factor of a three-layer Mu-metal tube from PTB. In the first case, the SQUID system has been operated in the BMSR in a setup that guarantees the highest possible resolution. In the latter case, the system operated in a totally unshielded environment. Furthermore, measurements inside the noise cancellation system of NPL are planned in the second period of 2014.

The developed measurement system and the obtained results should be used in upcoming projects, e.g. PTB will contribute with to a national project of the German company ILK, intended to develop new Helium bath cryostats.

A magnetic calibrating facility able to regulate temperature in the reduced range of -25 to 80 °C

A magnetic calibrating facility was built at CMI (with CTU collaboration) that can regulate temperature in the reduced range of -25 to 80 °C using a thermostatic 6-layer magnetic shielding. The shielding was characterised by a SQIUD magnetometer developed at PTB Berlin. The measurement confirms that the shielding layers do not add extra noise but remanence of the shielding can caused an influence on the measurement.

Calibration method of coil system was developed. The method is based on a scalar magnetometer and it can achieve precision of 200 ppm. The method was tested against national coil magnetic flux density standard. Additionally, the scalar calibration procedure was tested at PTB's magnetic calibration facilities within an ESRMG. The calibrating algorithm determined constants and orthogonalities of calibrated tri-axial coil systems.

CMI developed a technique for calibrating tri-axial magnetic sensors by using tri-axial Helmholtz coil system, and a scalar magnetometer. Nulling system or movement devices are not required. If tri-axial coils are calibrated, then parameters of tri-axial magnetometer are measured in this coil system by using developed principle. The calibration principle was verified in a suburban calibrating facility with 5nT p-p noise. The expanded uncertainty of 0.05 degrees was achieved during the calibration of the orthogonality. The magnetometer sensitivity was calibrated with an extended uncertainty of less than 450 ppm.

The uncertainty of used Overhauser magnetometer was established during the comparison APMP.EM-S14 "Earth-level DC magnetic flux density".

WP3: Metrology for Spin Torque Materials

Magnetic random access memories (MRAM) making use of the spin torque effect for programming the memory cells are presently seen as the only viable candidate to replace DRAM for embedded memories beyond the 10 nm node. Therefore optimised MRAM materials are required which need to be developed and texted using suitable metrology tools and methods. Therefore this WP has provided metrology tools and methods for wafer scale measurements of critical spin torque material parameters.

This WP has provided:

- A method for the fast and non-destructive inductive determination of key material parameters for Spin-Torque (ST) materials. It allows for the first time to determine the key material parameter of the ST critical current density in a lithography-free process.
- Metrology and simulation tools for inductive testing of magnetic thin film properties in the GHz range.

In this work package non-destructive inductive metrology for key parameters of spin torque (ST) materials based on magnetic multilayer stacks was developed and tested. With this metrology in particular the effective damping α, the saturation magnetisation M_S, the anisotropies H_K of the individual layers and the interlayer exchange couplings J_{FL} between the pinned and the free layer were be characterised. From these data, the critical current for spin transfer toque induced magnetisation switching, j_{c0}, can be calculated. In a first step, the theories for the determination of α_{eff} M_S, H_K and J_{FL} and for the calculation of j_{c0} based on the inductive characterisation of an MTJ sample for typical anisotropies and measurement geometries were compiled. To test the theory, α_{eff} M_S, H_K and J_{FL} of a set of MTJ test structures with different MgO barrier thickness t_{MgO} were determined from inductive measurements and the corresponding critical current densities were calculated. The CoFeB/MgO based MTJs with a wedge grown tunnel barrier layer were deposited by the collaborators Singulus Nanodeposition AG and Bielefeld University. The feasibility of the inductively derived j_{c0} was confirmed by current induced magnetisation switching (CIMS) data obtained on patterned nanopillars from the same material stack.

For the theoretical description the MTJs were modeled as a coupled two layer system consisting of a free layer (FL) with magnetisation $\boldsymbol{M}$ and saturation magnetisation M_S and a fixed layer as a reference layer with a magnetisation $\boldsymbol{M}_{fix}$. The FL has an in-plane uniaxial anisotropy K_u and, at zero external field, the system has two stable magnetic states of the two electrodes, parallel (P) and antiparallel (AP). For this geometry standard ST modelling yields:

$$j^{c0}_{P\to AP/AP\to P} = \mp 2\frac{e}{\hbar}\frac{\alpha_{eff}\, t_{FL}\mu_0 M_s}{\eta} H_{eff} \quad (1)$$

with a spin transfer efficiency η that can be calculated from TMR values (using Julliere's model), which are accessible via non-destructive wafer scale measurements. Thus, from the parameters α_{eff}, M_S, J_{FL} and K_u we can calculate j_{c0}.

A determination of these parameters is possible from non-invasive inductive techniques like VNA FMR or In a macrospin model, the precession frequency f_{FMR} of the magnetisation vector can be derived as an extended Kittel formula:

$$f_{FMR} = \frac{\gamma\mu_0}{2\pi}\sqrt{H_{ext}\cos(\varphi-\phi) + H_u\cos(2\phi) + H_{int}\cos(\phi)} \cdot \sqrt{H_{ext}\cos(\varphi-\phi) + H_u\cos^2(\phi) + H_{int}\cos(\phi) + M_S} \quad (2)$$

By fitting this model to the measured field dependence of f_{FMR} from the inductive measurements $H_{int} = J_{FL}/(t_{FL}\mu_0 M_S)$, $H_u=2K_u/\mu_0 M_S$ and M_S can be found. The effective damping α emerges from the linewidth of the FMR peak or the decay of the oscillation measured by PIMM, respectively.

The MTJ stacks studied for the comparison of CIMS and inductive measurements had a varying thickness of the tunneling barrier (t_{MgO}=0.62 to 0.96 nm) without changing the remaining stack.

CIMS measurements were performed on nanopillars with t_{MgO} = (0.96, 0.88, 0.82 and 0.71) nm and with voltage pulses of length 1 ms $\leq\tau\leq$54 ms. These measurements serve as a reference to validate the inductive measurements. The TMR and RA were determined by wafer scale measurements using a commercial current in-plane tunneling setup.

For inductive characterisation pieces of 2×4 mm^2 lateral dimension were cut from the MTJ wafer. PIMM measurements were performed at room temperature with easy axis external field. The MTJ stacks were placed on top of a coplanar waveguide (CPW) contacted with microwave probes. The setup can be used both for frequency domain and time domain inductive measurements. The measured field dependence of the FL precession frequency (open dots) was fitted by the model function in Eq. (2) (red line) to determine the FL magnetic parameters M_S, K_u and J_{FL} of the MTJ stacks. A constant magnetisation saturation of M_S=1.35 T is obtained for all samples. The results for J_{FL}, K_u and α_{eff} are summarised in Figures 15 and 16.

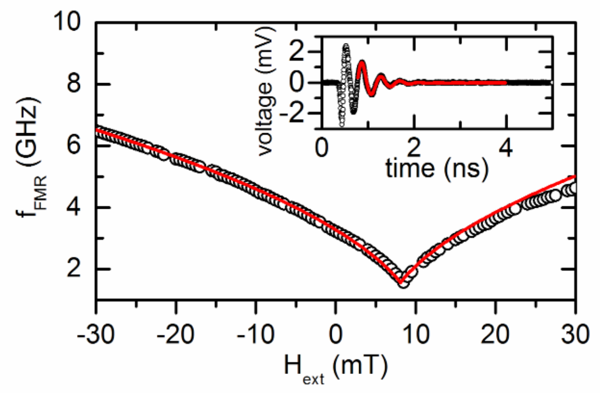

Figure 15: Static field dependence of f_{FMR} derived from PIMM for tMgO = 0.76 nm. Red line is the fit to Eq. (2). The inset shows the inductive PIMM data at 5mT easy axis field and the fit to a damped sinusoid (red).

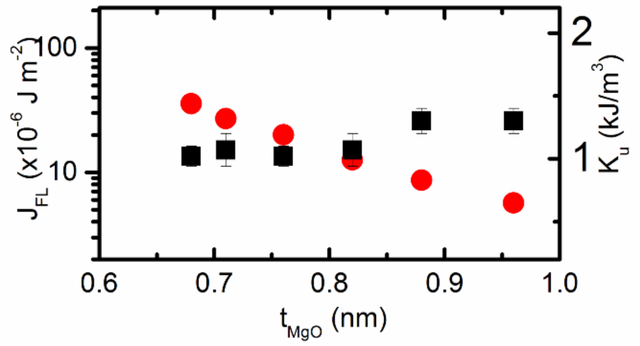

Figure 16: (Color online) MgO thickness dependence of the coupling J_{FL} between free and reference layer (red circles) and uniaxial anisotropy energy Ku of the free layer (squares) from PIMM measurements.

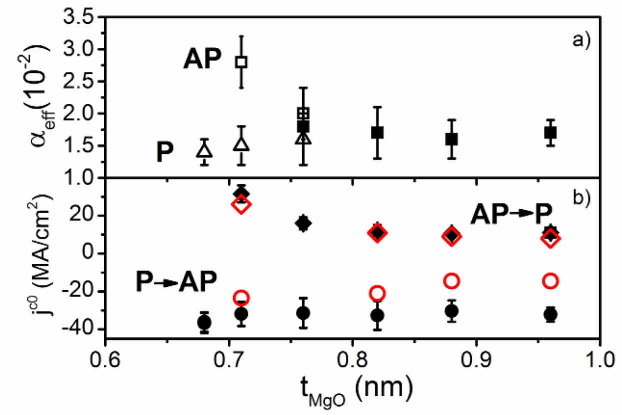

Figure 17: (a) effective damping α_{eff} vs. MgO thickness. Open triangles refer to the damping parameter at parallel (α_P), open squares to the damping parameter at antiparallel configurations (α_{AP}). Full squares to equal α_{eff} of both configurations. b) Inductively determined j^{c0} (black symbols) for P →AP ($j^{c0}_{P\rightarrow AP}$, circles) and AP→P ($j^{c0}_{AP\rightarrow P}$, rhombs) switching. Red symbols show j^{c0} as determined from CIMS experiments on individual nanopillars.

These inductively determined parameters were used to calculate the expected j_{c0} as a function of t_{MgO} as shown in Figure 17 (b). The black symbols mark the inductively determined values of j_{c0} for AP→P (full rhombs) and P→AP (full circles). The red open symbols mark the values of j^{c0} as determined from CIMS experiments on nanopillars fabricated from the same MTJ stack. For AP→P switching both data sets show an excellent agreement over the whole range of t_{MgO} confirming the feasibility of inductive determination of j_{c0}. For P→AP reversal a deviation of the two values beyond the measurement uncertainty is found for t_{MgO} > 0.85 nm. For the lower thickness range the inductive data of j_{c0} agrees better with the CIMS values. Note that also the general trends of the thickness dependence of j_{c0} of both data sets agreed well.

To summarise, the results of the inductively determined j_{c0} show a good agreement with the CIPT measurements opening the path towards a future inductive and non-destructive determination of this key STT material parameter. A publication on this work was submitted to IEEE Trans. Magn.

In a further task the above described inductive metrology was expanded to wafer scale non-destructive measurements. Therefore several inductive probe head prototypes suitable for local inductive probing of wafer scale ST materials based on a microfabricated coplanar wave guide (Figure 18) were developed. An optimised prototype initially was tested on single layer magnetic thin films [Probe Head Paper 1]. The head consisted of a CPW with rear contacts that can be brought in contact with the magnetic film on a wafer. In a second step, the probe head was used for a wafer scale inductive characterisation of ST materials. The results were validated by comparison to standard inductive metrology as described above.

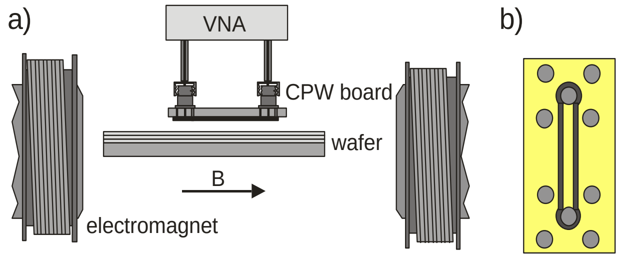

Figure 18: Schematic drawing of the experimental setup for wafer probing. a) The sample and the probe head are placed between the coils of an electromagnet generating the external field. FMR measurements are performed using a commercial VNA; b) schematic drawing of the probe head CPW board.

We compared inductive data from VNA-FMR measurements with the validated setup (S-FMR) with probe head (PH) data. A similar wafer was cut into pieces of (i) 20x20mm^2 (larger than the PH size) to test "wafer scale" measurements and (ii) 5x5 mm^2 size for characterisation by S-VNA. VNA-FMR measurements were performed using both setups. f_{FMR} and Δf of the frequency domain resonances peaks were calculated by fitting the sum of a symmetric and an antisymmetric Lorentzian to the respective data. α_{eff} was calculated from measured Δf.

A typical measurement result of f_{FMR} (a) and α_{eff} (b) is shown in Figure 19. The data is shown for negative applied fields $\mu_0 H$ and hence for AP configuration (full configuration of FL, fixed layer and bottom SAF layer is sketched). Note that our PH setup allows the application of higher fields and hence the wider PH data range. In the overlapping data range f_{FMR} obtained by S-FMR (red) and PH-FMR (black) agree well. Fitting f_{FMR} to Eq. 2 yielded a good agreement of magnetostatic parameters: PH-FMR: $\mu_0 M_S$=0.84±0.02 T, J_{FL}=1.3±0.1 µJ/m^2; S-FMR: $\mu_0 M_S$ =0.81±0.02 T, J_{FL} =12±1 µJ/m^2) with K_u set to 1200 J/m^3. Note that the present centimetre size PH in contact with the MTJ wafer revealed transmission discontinuities due to standing GHz waves inhibiting data analysis for certain frequencies (PH data gaps). When f_{FMR} approached these gaps the PH-FMR resonance data were no longer described by a Lorentzian and therefore, Δf derived from PH-FMR and hence PH-α_{eff} was artificially enhanced. The PH-FMR data shows a slightly lower damping in the centre of the accessible data ranges and a strong increase of α_{eff} when f_{FMR} approached frequency gaps. Averaging over the displayed data yielded α_{eff}=0.04±0.01, a comparable value for the S data, but with larger uncertainty.

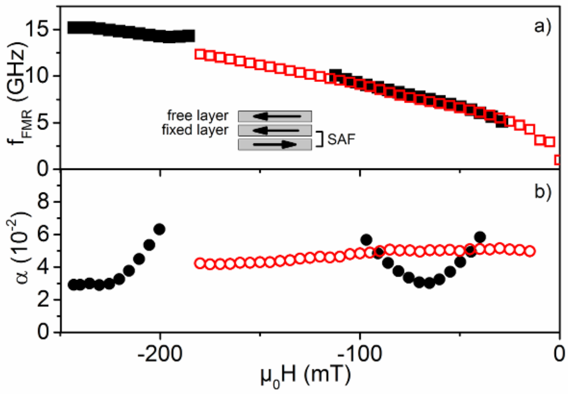

Figure 19: (a) f_{FMR} vs. H measured by the inductive probe head (PH, black) and standard VNA-FMR (S, red open). Magnetic configuration is sketched. (b) α_{eff} as calculated from the linewidths of the resonance peaks from PH (black) and S (red open dots) measurements.

These results demonstrated the feasibility of a wafer scale FMR for the determination of key material parameters for STT MRAM. For future low uncertainty probing of j_{c0} further optimised probe heads are being developed to avoid detrimental CPW resonances. They include bendable CPWs on a flexible substrate with reduced contact area to the stack and a larger distance to the high frequency connectors and rigid CPWs with spatially varying CPW geometries. Such wafer scale probing of spin torque material properties will in the future allow highly efficient development and in-line testing of industrial spin torque materials.

WP4: Micromagnetic numerical modelling

The development of advanced magnetic sensors is more and more relying on models predicting the magneto-resistance response of the sensor prior to production of the first sensor prototype. Such models are based on numerical finite element codes that derive the magnetic domain structure from minimizing the magneto-static and exchange energy of the system. Therefore this WP has addressed the standardisation of such micromagnetic modelling to increase the model reliability for the stakeholders.

This WP has provided:

- Validated modelling tools for the micromagnetic modelling of micro- and nano-scale magnetic thin film sensors have been developed. They allow reliable modelling of the most important magnetic sensor device properties including magnetic domain structure, magnetisation reversal curves, magneto transport properties and sensitivity.

Standardisation of micromagnetic numerical tools

The objective of this Work Package was the development of an advanced micromagnetic numerical code for the efficient solution of the Landau-Lifshitz-Gilbert (LLG) equation in large-scale magnetic nanostructures and patterned films, for potential applications as magnetic sensing elements. After its validation, the code was extensively applied to provide a theoretical interpretation of the experimental results obtained along the project, especially in WP1 and WP5.

The development of the micromagnetic solver required a preliminary phase of optimisation and test on ad-hoc standard problems, devoted to the individuation of the most reliable and efficient numerical techniques for the spatial and time discretisation of the LLG equation. In this context, particular care was taken in the spatial integration of both quantum-mechanical exchange coupling and magnetostatic or long-range interactions. In parallel, several time integration schemes were tested to find the most efficient one in terms of numerical stability and computational performance. After this phase, the micromagnetic solver developed at INRIM was validated by comparison to OOMMF code, produced by the Micromagnetic Modelling Activity Group of National Institute of Standards and Technology (NIST), US [1]. Additional tests were carried out by comparison to MuMax code, developed by the Department of Electrical Energy, Systems and Automation of Ghent University, Belgium [2].

The final version of INRIM micromagnetic code implemented original numerical techniques, coupling a fast multipole method for the magnetostatic field computation in large-scale media [3], with a Finite Difference technique for the spatial reconstruction of the exchange field on non-structured meshes [4]. This simulation tool is particularly suitable for handling large patterned media, as dot/antidot arrays, also in the presence of complex lattice structure (e.g. dots/antidots with irregularly curved boundaries) and heterogeneous material composition. In detail, the patterned medium is decomposed into a macroscale grid of cells, in turn discretised into a non-structured mesh having average size comparable to the exchange length. Locally, the magnetostatic field is the sum of a short-range term, computed by discretising Green integral equation over a limited region, and a long-range term, which represents the contributions of far macrocells as a set of multipole moments. The second order derivatives in the exchange field are calculated by defining a Taylor series expansion around each computational point and by solving a over-determined set of linear equations through norm minimisation. To preserve the magnetisation amplitude and enable the efficient calculation of equilibrium states, the time discretisation of the LLG equation was performed by means of a geometric integration scheme based on Cayley transform [5].

The INRIM micromagnetic solver was further optimised through the development of a parallelised version able to run on graphical processing units (GPUs) [6]. The high-performances of the parallelised solver were tested by comparison to the CPU version in the calculation of the hysteresis loops of large patterned magnetic films, e.g. arrays of bi-component dots with 300 nm diameter (the magnetisation spatial distribution at the coercive field for an 8×8 array is reported in Figure 20 (a)). Figure 20 (b) compares the elapsed time for the simulation of one time step as a function of the number of dots composing the patterned film, for an average mesh size of 7 nm. The curve associated to the CPU implementation rapidly increases with the dot number; for an 8×8 array the ratio between CPU and CPU-GPU elapsed time is ~75. The increase in computational time with mesh refinement in the CPU-GPU implementation is plotted in Figure 20 (c).

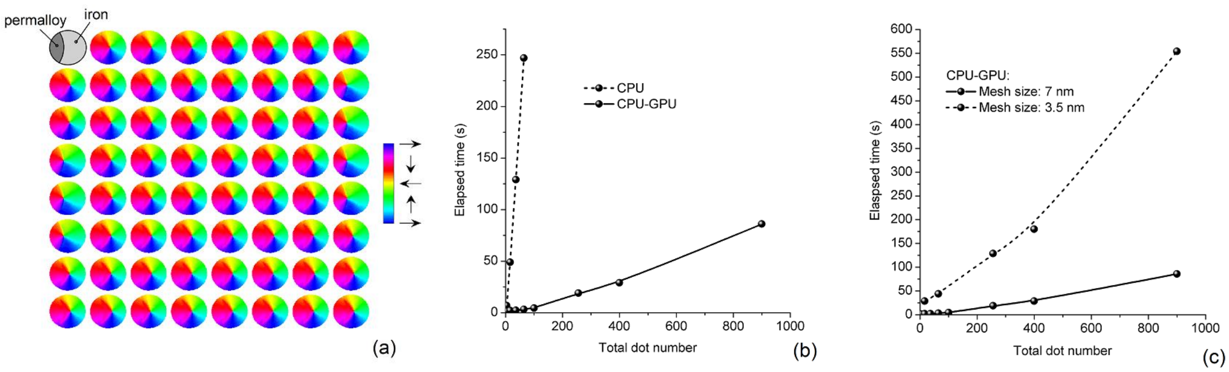

Figure 20: (a) Magnetisation spatial distribution at the coercive field for an array of 8×8 bi-component dots and an external field applied along y-direction. The color scale identifies the magnetisation angle (in degrees) with respect to x-axis. Elapsed time for the simulation of one time step as a function of the number of dots in the patterned film: (b) comparison among CPU and hybrid CPU-GPU implementation; (c) comparison among CPU-GPU simulations for two values of the mesh size.

[1] http://math.nist.gov/oommf/
[2] A. Vansteenkiste and B. Van de Wiele, *"MuMax: a new high-performance micromagnetic simulation tool"*, J. Magn. Magn. Mat. 323, pp. 2585-2591 (2011)
[3] A. Manzin and O. Bottauscio, *"Multipole expansion technique for the magnetostatic field computation in patterned magnetic films"*, J. Appl. Phys. 111, 07D125 (2012)
[4] O. Bottauscio and A. Manzin, *"Spatial reconstruction of exchange field interactions with a finite difference scheme based on unstructured meshes"*, IEEE Trans. Magn. 48, pp. 3250-3253 (2012)
[5] A. Manzin and O. Bottauscio, *"A micromagnetic solver for large-scale patterned media based on non-structured meshing"*, IEEE Trans. Magn. 48, pp. 2789-2792 (2012)
[6] O. Bottauscio and A. Manzin, *"Parallelized micromagnetic solver for the efficient simulation of large patterned magnetic nanostructures"*, J. Appl. Phys. 115, 17D122 (2014)

Modelling of thermal effects

The objective of this task was the extension of the micromagnetic simulation tool developed at INRIM to thermal effects, to arrive at a complete model of magnetic devices under realistic operative conditions. At the sub-micrometer length scale, switching processes can be strongly influenced by the magnetisation fluctuations induced by thermal agitation, which can affect coercive field and switching time.

Thermal effects were included in the micromagnetic solver following the Langevin approach: an isotropic, spatially and temporally uncorrelated Gaussian white-noise term was introduced to simulate the interaction between magnetisation and lattice vibrations. In particular, the thermal effects were included in the Landau-Lifshitz-Gilbert (LLG) equation by adding a fluctuating field $\boldsymbol{H}_{th}(\boldsymbol{r}, t)$ to the effective field. The amplitude of $\boldsymbol{H}_{th}(\boldsymbol{r}, t)$ was derived from the fluctuation dissipation theorem, namely:

$$\mathbf{H}_{th}(\mathbf{r},t) = \boldsymbol{\eta}_{th}(\mathbf{r},t)\sqrt{\frac{2\alpha k_B T}{\gamma\mu_0 M_S \Delta s^3 \Delta t}} \qquad (3)$$

where T is the absolute temperature, k_B is the Boltzmann constant, γ is the gyromagnetic ratio, V is the magnetic nano-object volume, M_S is the saturation magnetisation, α is the damping coefficient, Δs is the average length of the spatial discretisation, Δt is the time step used in the numerical algorithm and $\boldsymbol{\eta}_{th}(\boldsymbol{r},t)$ is a stochastic vector whose components are Gaussian random numbers, uncorrelated in space and time.

The extended version of the micromagnetic solver was tested focusing on the criticalities that arise in finite temperature simulations, such as:

- the dependence on the average size Δs of the mesh used to discretise the sample;
- the reaching of stable solutions only for very low time steps Δt;
- the need of computing several stochastic realisations, from which extracting average values.

As an example, Figure 21 (a) shows a test case in which a permalloy square dot with lateral size of 75 nm and thickness of 10 nm, initially saturated along *x*-axis, is subjected to an external field of 10 kA/m, applied along the opposite direction. The graph compares the magnetisation dynamics calculated when neglecting thermal effects and for a temperature of 300 K, considering several stochastic realisations. The simulations were made by introducing a spatial discretisation of 5 nm and a time step of 50 fs. The influence of time step and spatial discretisation size is put in evidence in Figure 21 (b), which reports the relaxation time (averaged over 15 stochastic realisations) as a function of Δs and Δt, for different values of absolute temperature T.

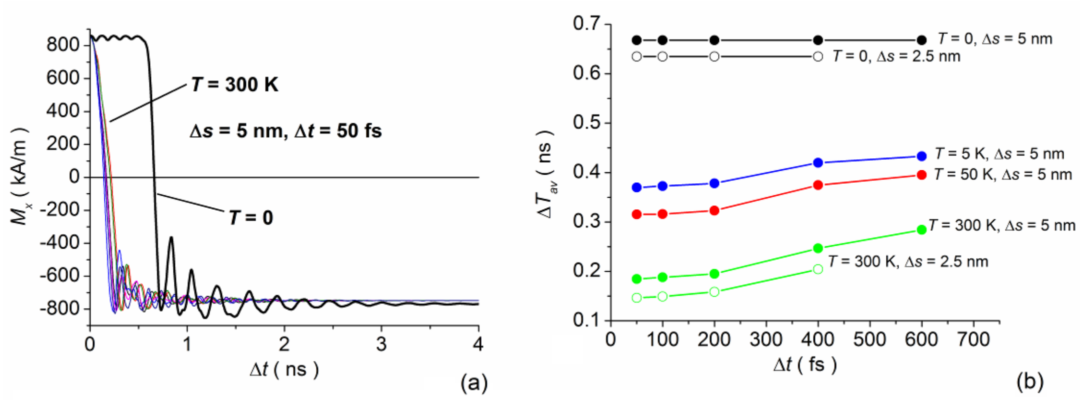

Figure 21: (a) Time evolution of the average x-component of the magnetisation, computed by considering a spatial discretisation of 5 nm and a time step of 50 fs. (b) Relaxation time (averaged over 15 stochastic realisations) as a function of Δs and Δt, for different values of the absolute temperature T.

Modelling of AMR sensor elements

The objective here was the micromagnetic modelling of the magnetisation processes in artificially patterned magnetic films exhibiting anisotropic magnetoresistance (AMR) effect. The attention was focused on magnetic antidot arrays as promising candidates for next generation AMR sensors. Antidot structure, which consists of a mesh of nonmagnetic inclusions (holes) embedded in a continuous magnetic film, introduces local demagnetizing fields that can strongly influence magnetisation reversal, shape anisotropy and magnetic domain configuration. In this case, the magnetoresistance response is a complex function of the external field orientation and its interpretation requires a detailed knowledge of the induced easy/hard axis directions and of the magnetisation spatial distribution. A powerful tool for the analysis of these aspects can be provided by ad-hoc micromagnetic and magnetotransport modelling.

To this aim, a numerical approach was developed at INRIM for the simulation of anisotropic magnetoresistance (AMR) phenomena in magnetic nanostructures, by coupling the micromagnetic code realised in Task 4.1 with a transport model for the determination of current density distribution. In the transport model, the AMR effect (deriving from the anisotropic scattering of conduction electrons due to spin-orbit interaction) was described by introducing a spatially-dependent electrical conductivity, which depends on the mutual orientation of magnetisation and current density vectors.

The developed micromagnetic-magnetotransport code was applied to analyse the magnetic domain configuration, the magnetisation reversal mechanism and the AMR behaviour of antidot arrays with different lattice configuration [1-3]. In connection with WP1, the code was extensively employed to interpret the experimental results (magnetic force microscopy images, quasi-static hysteresis loops and magnetoresistive curves) obtained on patterned permalloy films fabricated at INRIM with different techniques. In particular, the attention was focused on antidot arrays prepared by electron-beam lithography (with hexagonal and rhombic lattice configurations) as well as by self-assembling of polystyrene nanospheres. In both cases, a very good agreement between simulations and measurements was obtained, enabling an insightful description of the magnetisation reversal processes and of their role in determining the field dependence of the AMR effect.

To simulate magnetisation processes in antidot arrays prepared by electron-beam lithography, which are generally characterised by an ordered lattice structure, periodic boundary conditions were imposed on the unit cell edges. The equilibrium domain patterns of both hexagonal and rhombic antidot arrays were calculated as a function of the external field, which was applied along two orthogonal directions, one parallel and one perpendicular to the electrical current used to probe AMR. On the scale range of the array unit cell, the simulations were in very good agreement with the MFM images, showing a leaf-type pattern around each hole. This is well demonstrated by Figure 22, which compares the calculated and measured remanent states for a 30 nm thick rhombic array film with a hole diameter of 480 nm and centre-to-centre distance of 1 μm.

The developed micromagnetic-magnetotransport code was also used to determine the magnetoresistance curves for both longitudinal (magnetic field parallel to electrical current) and transverse (magnetic field perpendicular to electrical current) configurations. As an example, Figure 23 reports the calculated AMR curves for a 30 nm hexagonal array film with hole diameter of 320 nm and centre-to-centre distance of 500 nm, together with the magnetisation maps at the equilibrium points immediately before and after the reversal.

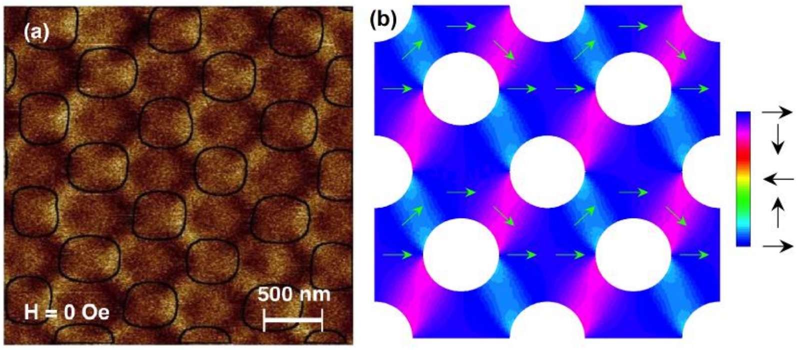

Figure 22: MFM image at remanence (a) of a permalloy antidot array with rhombic lattice prepared by electron-beam lithography and corresponding simulated magnetisation map (b). The colour scale identifies the magnetisation angle (in degrees) with respect to x-axis.

When simulating the magnetisation processes in antidot arrays prepared by self-assembling, the intrinsic disorder was modelled by introducing randomly distributed unpatterned areas in a representative sample (with size in the order of 6 μm). To improve computational performances, the magnetostatic field was calculated by adopting the fast multipole method. The comparison between experimental and simulated results leaded again to a very good agreement, enabling to understand the role of lattice disorder on the magnetisation reversal mechanisms. As can be observed in Figure 24 (a), which shows the simulated AMR curves for a 30 nm antidot array with hole diameter of ~330 nm and centre-to-centre distance of ~500 nm, the presence of disorder produces a variation of the magnetoresistance signal of the same amplitude for longitudinal and transverse configurations. This is a consequence of the decrease in the shape anisotropy contribution due to the more disordered distribution of nonmagnetic inclusions, which lead to more complex magnetisation patterns, as shown in Figure 24 (b).

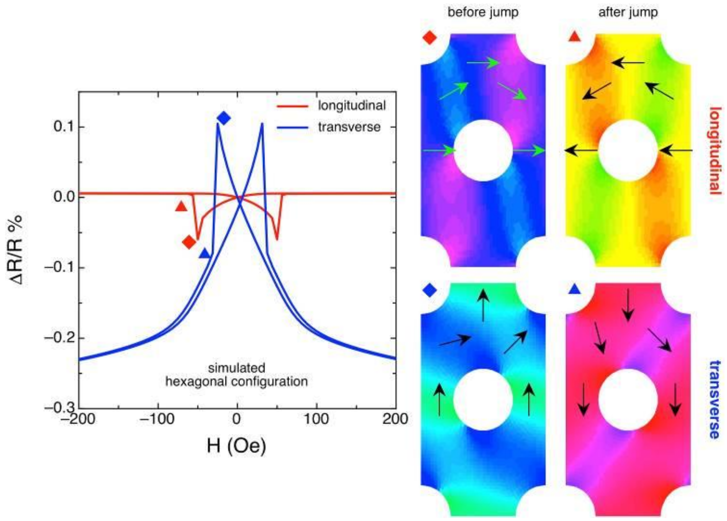

Figure 23: Simulated AMR curves for a hexagonal antidot lattice prepared by electron-beam lithography. On the right: simulated magnetisation maps are reported for both configurations for the equilibrium points immediately before and after the irreversible jumps.

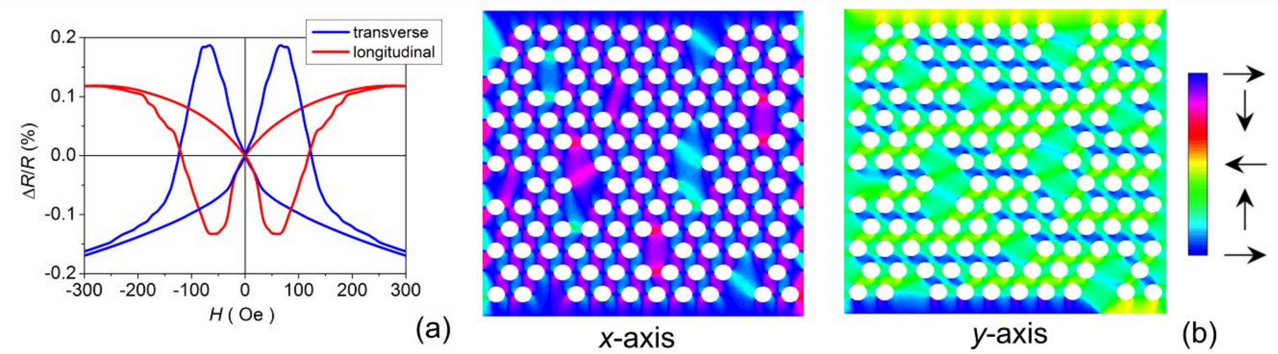

Figure 24: (a) Simulated AMR curves for an antidot array with intrinsic disorder. (b) Simulated magnetisation maps at the remanent state after saturating the film along x- and y-axis directions.

[1] Manzin and O. Bottauscio, *"Micromagnetic modelling of the anisotropy properties of permalloy antidot arrays with hexagonal symmetry"*, J. Phys. D: Appl. Phys. 45, 095001 (2012)

[2] B. Van de Wiele, A. Manzin, A. Vansteenkiste, O. Bottauscio, L. Dupré, and D. De Zutter, *"A micromagnetic study of the reversal mechanism in permalloy antidot arrays"*, J. Appl. Phys. 111, 053915 (2012)

[3] M. Coïsson, A. Manzin, G. Barrera, F. Celegato, E. Enrico, P. Tiberto, and F. Vinai, *"Anisotropic Magneto-Resistance in $Ni_{80}Fe_{20}$ Antidot Arrays with Different Lattice Configurations"*, submitted to Applied Surface Science.

Modelling of devices based on domain wall control

The objective of this task was the micromagnetic modelling of magnetoresistive sensors based on domain wall (dw) control, as a support to the interpretation of the experimental results (magnetoresistance measurements and magnetic force microscopy images) obtained in WP5. In particular, the micromagnetic-magnetotransport model developed at INRIM was extensively employed to simulate magnetisation dynamics and anisotropic magnetoresistance (AMR) behaviour of L-shaped permalloy nanowires, as promising candidates for both sensing and magneto-logic applications. The attention was focused on magnetic nanostructures fabricated at PTB and further characterised at NPL, analysing the influence on the magnetoresistance (MR) signal of the magnitude and orientation of the external field as well as of the nanowire width and geometry. A very good agreement between measurements and simulations was found, enabling the individuation of the optimal working conditions and nanostructure geometry for the design of sensing elements with improved features [1].

The MR response of the device was first studied in dependence on the magnitude and angular orientation β of the applied magnetic field (in-plane) with respect to one of the nanowire arm (see inset of Figure 25 (a)), considering a 25 nm thick device with 150 nm width nanowires, ending in 1 μm diameter disks. As an example, Figure 25 (a) and (b) show the computed and measured MR curves associated with major hysteresis loop, when β is equal to 10° and -5°, respectively. Very satisfactory correlation of the experimental and modelling results was found for practically the entire field range, supporting the conclusion that MR properties in permalloy nanowires are mainly dominated by the AMR effect.

The field-dependence of the MR behaviour was inferred by analysing magnetic domain configurations at relevant equilibrium points, whose schematic representations from micromagnetic simulations are reported on the bottom of Figure 25. The schemes illustrate how for the positive field orientation the remanent state is characterised by dw confinement at the device corner, followed by dw depinning (resistance decrease) and then by dw pinning (resistance increase). For the negative field orientation no dw is present at the corner at remanence and the first switching event is characterised by dw pinning, followed by dw depinning. The role of circular disks in promoting dw pinning and depinning phenomena is put in evidence in Figure 25 (c), which shows the formation of vortex state in the disks at remanence.

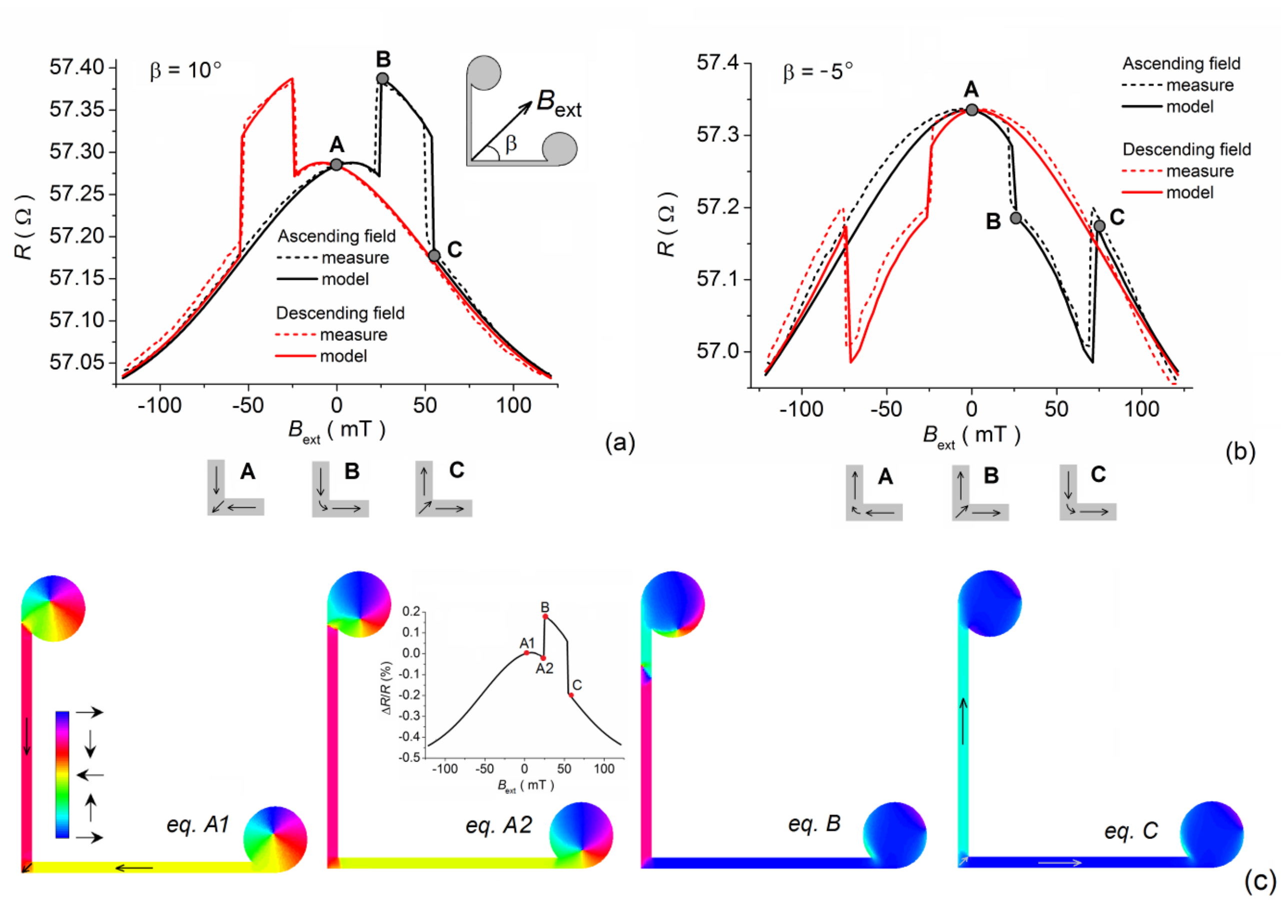

FIGURE 25: Simulated and measured AMR response of a 150 nm width device for a field applied at an angle β of 10° (a) and -5° (b). (c) Simulated spatial distributions of the magnetisation at specific equilibrium points shown in the MR curve (inset) for β = 10°. The colour scale identifies the magnetisation angle (in degrees) with respect to x-axis.

It was also demonstrated how the dw pinning/depinning fields are strongly influenced not only by the external field orientation, but also by the nanowire width *w* (see Figure 26 (a)). The role of corner shape was further investigated, showing that for positive field angular orientations, the remanent state is generally characterised by a vortex-like magnetisation configuration in proximity to the corner (not present in the 75 nm width device, due to volume reduction). This effect can be seen in Figure 26 (b).

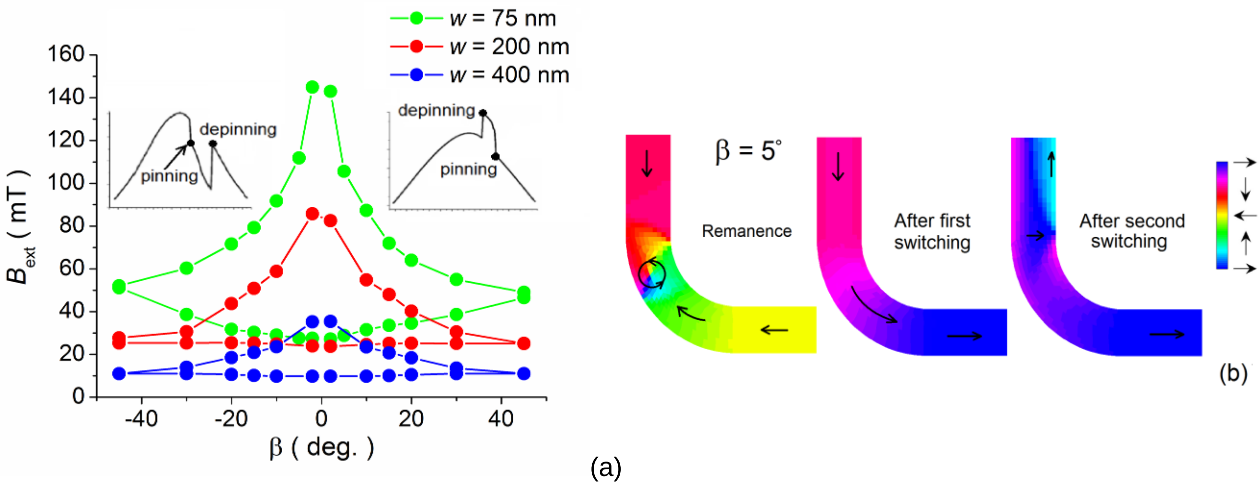

FIGURE 26: (a) Computed dw pinning and depinning fields as a function of the angular orientation of external field β and of the device width w. (b) Equilibrium magnetisation spatial distributions at the corner of a rounded device at remanence and after irreversible jumps for $\beta = 5°$ and w = 200 nm.

[1] Manzin, V. Nabaei, H. Corte-León, O. Kazakova, P. Krzysteczko, and H.W. Schumacher, *"Modeling of Anisotropic Magnetoresistance Properties of Permalloy Nanostructures"*, IEEE Trans. Magn. 50, 7100204 (2014).

WP 5: Metrology for Advanced Magnetic Sensor Concepts

New concepts for next generation magnetic sensors are in the R&D stage at European research laboratories and industrial development centers. Among the promising candidates for next generation high performance sensors are ultra-high integrated Hall sensors and magnetic domain wall (DW) based magnetic nano-sensors. Therefore this WP has provided underpinning metrology for development, testing, and R&D of micro-Hall and DW sensor devices.

This WP has provided:

- A metrology system for the characterisation of novel magnetic domain wall sensor devices. The system allows accurate and complete mapping of the domain wall-related change in the anisotropic magnetoresistance as a function of the magnitude and orientation of the applied magnetic field. It allows identifying highly reproducible transitions between domain states and hence to determine the optimal working parameters to underpin the development of specific novel domain wall sensor devices.
- A new micro Hall sensor based method for the calibration of the magnetic stray fields of magnetic near field probes for magnetic force microscopy (MFM). It will in the future allow MFM bases traceable measurements of magnetic stray field on the nano scale with strong implications device testing and materials research.

Micro-Hall devices

Epitaxial graphene on SiC substrate presents an alternative route to conventional semiconductors for development of ultra-sensitive Hall detectors. The material allows for improved coupling due to the reduced vertical distance between the active channel and magnetic nano-object. Additionally, a general trend for miniaturisation of both sensors and magnetic label (bead) leads to a fundamental challenge of reliable detection of a true magnetic signal and its separation from parasitic signals, for example, generated by inductive couplings, foreign ferromagnetic materials in the vicinity of the device, etc. Within MetMags project, we have demonstrated that at room temperature epitaxial graphene magnetometers approaching that of state-of-the-art semiconductor devices of a similar carrier density and size. We have also established that epitaxial graphene devices offer lower resistivity and an order of magnitude better sensitivity to magnetic field, when compared to CVD graphene Hall sensors.

Micron-sized Hall sensors made of epitaxial graphene grown on 4H-SiC(0001) have been fabricated and studied at room temperature using transport and noise spectrum measurements. Bead positioning was performed using a nano-manipulator inside of the FIB system (Figure 27, left). We reported detection of 1-µm Dynal bead with the magnetic moment of 4×10^{8} μ_B, using a 2 µm-epitaxial graphene device. A phase-sensitive AC-DC Hall magnetometry method developed by NPL was used to reliably detect the bead with a large response of V_{AC}~7 µV (Figure 27, right).

By comparison with our previous results where the same type of bead was detected using InSb devices, graphene sensors demonstrate a significantly larger output in the AC Hall voltage, owing to better coupling to the bead in the vertical direction and improved current stability due to more efficient energy loss rate for hot carriers in graphene. Thus, we demonstrate a considerably improved performance and durability of graphene Hall sensors as compared to the standard semiconductor devices. These properties of graphene devices are highly important for their use in metrological application and as biological and environmental detectors.

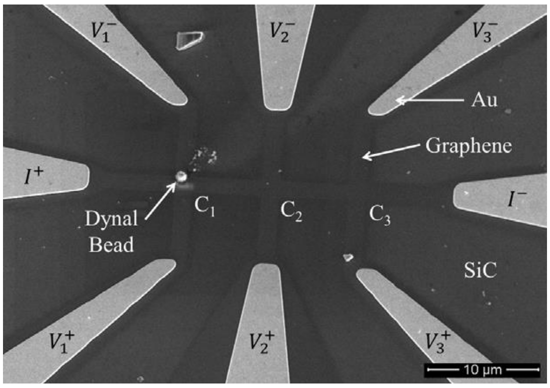

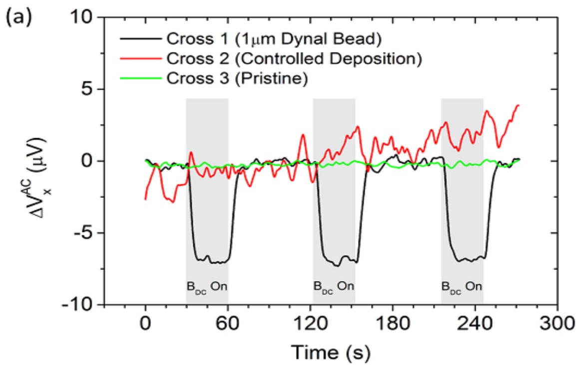

Figure 27: Left: SEM image of a 1 µm- Dynal bead on cross 1 of 2 µm-wide epitaxial graphene device. Right: In-phase component of the AC Hall voltage in response to 30 s long steps of DC magnetic field.

Domain wall based sensors

We have developed a method for detailed mapping of resistance in domain-wall based nanosensors allowing for precise correlation of their magnetisation state and changes in magnetoresistance (MR). Such devices have promising applications, *e.g*. as MR sensors for magnetic bead detection. The direct comparison is possible due to a simple magnetic state of the device comprised from single/double domains and characterised by absence/presence of a domain wall (DW), which can be pinned/depinned at the corner of the nanostructure. By varying the orientation of the external magnetic field, we identified the angular dependence of the DW pinning and depinning fields. For angles $0°<\beta<90°$ ($180°<\beta<270°$), the change of the resistance is characterised by the depinning of the DW from the device corner, followed by nucleation of another DW in the disk and pinning at the corner. An opposite behaviour (pinning followed by depinning) is found for $90°<\beta<180°$ ($270°<\beta<360°$). We show that whichever switching event (pinning or depinning) occurring first it has a small angular dependence, while the second switching event is characterised by a significantly stronger angular dependence (Figure 28, symbols).

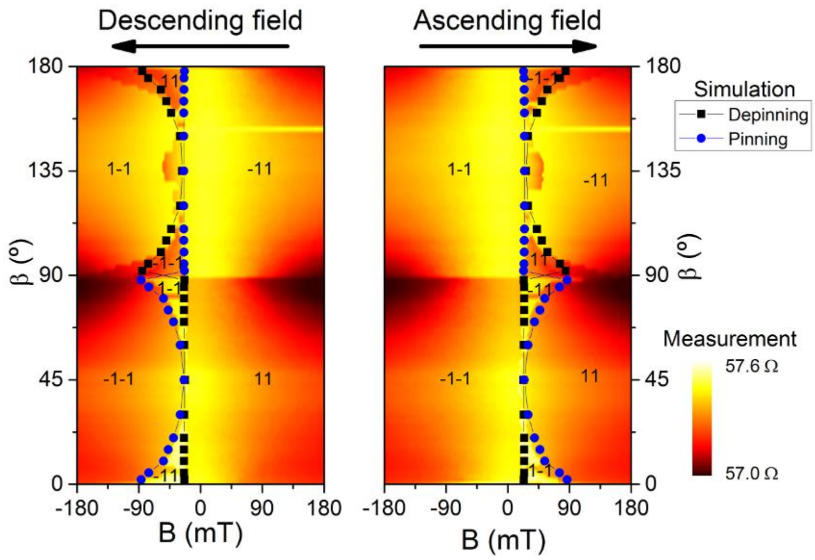

Figure 28: 2D maps of the AMR dependence on the angular orientation β and the magnitude of the external magnetic field. The field sweeps from a high positive to a high negative value (left) and vice versa (right). The calculated DW pinning/depinning fields are identified by square and dot symbols, as specified in the legend.

By varying the field magnitude and orientation, we plot 2D maps of the device MR (state space maps), which allow for a clear identification of four main magnetisation configurations characterised by the presence/absence of the DW (Figure 28, colour maps). The boundaries between different states, characterised by sharp resistance jumps, correspond to abrupt changes in the domain configuration. Whereas majority of transitions between the states occurs through a sharp boundary demonstrating regular and reproducible transitions between the main states, some of them characterised by an increased probability of stochastic switching. The first type of transitions is clearly the most suitable for sensing applications. Using the state space maps, it is possible to identify DW pinning and depinning fields. Such state space maps are extremely useful for determination of working parameters, such as the minimum field needed to switch both arms at different device orientations, or the most appropriate angle for maximal separation of the pinning and depinning fields. Thus, space maps are extremely helpful for establishing of the best conditions for sensing applications.

A complete state space map also allows for prediction of the DW evolution under an external magnetic field which varies both in magnitude and orientation without need of repeating MR or MFM measurements. These predictions were tested experimentally against real magnetotransport measurements with the results showing a very good experimental agreement. These findings are essential for the reliable initialisation of arrays of DW sensors into a well-specified sensing state.

4 Actual and potential impact

All the new calibration facilities and metrology tools and methods which have been delivered by the project will enable the European magnetic sensor industry to develop, produce and calibrate more reliable magnetic sensors to stay competitive in the global market. Already during the course of the project early uptake of project results by industry has occurred generating a significant intermediate impact. Further impact has been achieved by various dissemination activities:

Dissemination activities

- A first stakeholder workshop has been organised in the framework of a UK Magnetics Society Seminar "Novel Magnetic Sensors", at NPL on 12 January 2011.
- A second stakeholder workshop entitles “New trends in magnetic field sensing” was held at INRIM, on 13 December 2012.

- A special session on Magnetic Sensor Metrology has been organised at the “European Magnetic Sensor and Actuator Forum” (EMSA) on 4-7 July 2012 in Prague with five speakers from the consortium. This session allowed dedicated dissemination to the European magnetic sensor R&D experts.
- An invited talk on “Magnetic Sensor Metrology” was given by the coordinator on the 12th MR Sensor Symposium in Wetzlar on 19th and 20th March 2013. This allowed high level focussed dissemination of the project results to about 150 stakeholders from the European MR sensor R&D and industry among them representatives of all major magneto resistive sensor manufacturers.
- A *Best Practice Guide* “Generation and measurement of DC magnetic fields in the magnetic field range of 1 nT to 1 mT” has been published as an NPL report (Mat 65) and is available online. This will benefit companies and institutes who have been sent the guide both now and in the future as the content will act as reference material when training future scientist. The guide can be seen as a first step towards future standardization. Copies have been sent to various industrial stakeholders. The guide can be downloaded via:

  http://resource.npl.co.uk/cgi-bin/download.pl?area=npl_publications&path_name=/npl_web/pdf/ mat65.pdf
- A large number of peer reviewed papers on the project output have been published in international scientific journals (see list of publications below). In addition more than 80 talks and posters have been presented at various relevant scientific conferences to disseminate the output of the project.
- Various standardisation committees and scientific bodies have been regularly updated on the outcome of the project, among them IEC TC 68 "Magnetic alloys and steel", EURAMET TC EM, and Deutsche Physikalische Gesellschaft (AK Magnetismus). Routes towards future uptake with respect to standardisation have been discussed.
- Consultation with stakeholders at the first stakeholder event allowed to define the temperature range required for the new variable temperature calibration capability at NPL. The industry requirement of -55 °C to 125 °C has been implemented. This exceeded the deliverable requirement of -40 °C to 100 °C.
- With substantial use of new measurement and calibration facilities developed within the project, an international comparison measurement of the earth magnetic field has been successfully completed. It allowed the validation of novel measurement infrastructure and will lead to improved CMCs at some of the participating European NMIs.
- Within the project, PTB Berlin has developed a measurement system which enables one to measure the flux noise down to very low noise levels. It is suitable to characterise the noise floor induced by samples or noise cancellation systems. This measurement system and the obtained results will be used in upcoming projects. For example, PTB will contribute to a national project of the German company ILK, intended to develop new low-noise Helium bath cryostats. In addition, PTB offers an up to three-day hands-on training course which teaches the basics in SQUID handling and SQUID characterisation.
- Publicity documents announcing the new capabilities have been sent to industries with an involvement in magnetic field measurements and related technologies
- Presentation of the key outcome of all work packages at EMSA 2014. At this conference the Best Practice Guide was displayed and this resulted in request for copies to be sent.
- Traceable calibration facilities for sensor calibrations in temperature range -25 to 80 °C at CMI. These calibration facilities allow calibration of sensors used in high temperature industrial applications like industrial motors, in geological exploration and space applications and hence directly impact these fields.

Early impacts and uptake

- A world leading anisotropic magneto resistance (AMR) sensor producer has optimised their magnetic thin film deposition and fabrication process based on magnetic force microscopy in variable magnetic fields at PTB. The new metrology system enabled the manufacturer to pinpoint the generation thin film point defects occurring during a passivation process in the production line. The manufacturing process was subsequently optimised and the defect generation was overcome.

- The low magnetic field facility at NPL has been used to measure the magnetic moment of components for the ESA EarthCARE mission. The total magnetic moment of the spacecraft is required to meet a certain value of magnetic moment to deliver the science quality of the mission objectives. If this is not achieved it is known that the science quality is deteriorated and that the full potential of the mission is not delivered at great expense to the EU.
- The European Space Agency ESA has expressed a strong interest in the best practice guide for magnetic field measurements (see dissemination activities) for their critical magnetic cleanliness work for future space missions.
- The low magnetic field facility at NPL has so far been used for industrial magnetic sensor calibrations by six European sensor producers. These included Bartington Limited and NXP.
- The new 3D magnetic field calibration systems at CMI have been used for industrial precision calibrations by a company for geological exploration.
- The newly developed scalar calibration method using the Overhauser magnetometer was successfully used for coil calibrations at the Adolf Schmidt Observatory for Geomagnetism, in Niemegk, Germany.
- Within the project, PTB Berlin has developed a measurement system which enables one to measure the flux noise down to very low noise levels. It is suitable to characterise the noise floor induced by samples or noise cancellation systems. This measurement system and the obtained results will be used in upcoming projects. For example, PTB will contribute to a national development project of a German company aiming at developing new ultra low-noise Helium bath cryostats.
- The new capabilities established along with the Best Practice Guide will continue to generate impact in the future. It is expected that these facilities will need further development to meet future industry needs and the capabilities now in place will provide an excellent platform to meet these expectations. An example is the need to consider temperature gradients and temperature shocks when characterising magnetometers.

Longer-term impacts

The present and future uptake of project outputs will lead to further long term economic and social impacts.

Impact on European industry and economy: The fast development of magnetic sensors as a key technology for wide spread future applications and high-tech products is highly beneficial for the advancement of the European high-technology industry and, hence for future employment in this sector. Europe traditionally has a strong industrial sensor branch and two of the three world leading vendors of AMR and GMR sensors are European based. However, the EU MR sensor industry faces strong international competition as well as fast product development which requires underpinning metrology to enable sustainable innovation in the EU. Direct access for EU MR sensor manufacturers to the new high level metrology infrastructure at the European NMIs gives a competitive edge to the European MR sensor industry in global competition.

Impact on consumer safety: Road accidents are a major cause of death in industrial countries. However automotive safety systems like anti-blocking brake systems (ABS) and electronic stability control (ESC) drastically reduce the likelihood of accidents. According to eImpact (2020 high scenario) ESC is expected to prevent by far the most fatalities and injuries: about 3,000 fatalities (-14 %), and about 50,000 injuries (-6 %) per year. Therefore, EC regulation No 661/2009 requires ESC systems on all vehicles from Nov. 1st 2014. Both ABS and ESC systems heavily rely on multiple magnetic sensor input (e.g. speed, rotation, acceleration and steering wheel position). Furthermore, magnetic sensors are nowadays used to monitor tire pressure, to control airbags or to detect whether seats are occupied and safety belts are in use. Therefore by providing enabling metrology for the development of improved magnetic sensors the project underpins the development of improved magnetic sensors with direct impact on traffic safety in Europe and worldwide.

Impact on health: In bio-technology monitoring the kinetics of protein interactions on a high-density sensor array is vital to drug development and clinical diagnostics. The current gold standard for these applications is based on surface plasmons but the detection threshold and the throughput are limited. Here, advanced and highly sensitive MR nanosensor arrays based on MR sensor devices have prospects for high throughput and the highest sensitivity to enable faster drug development and fast, cheap and reliable clinical diagnostics. Other health relevant applications of MR sensors are cardiac pacemakers and magnetic nanoparticle detection for cancer diagnosis and treatment. Again, the new metrology infrastructure at the European NMIs as well as improved measurement guidelines as provided by this project allows better sensor calibration for improved bio-tech and health applications.

Impact on science and innovation in the EU: The project has carried out excellent, cutting edge research at European NMIs in collaboration with European industry and European universities in a highly competitive field. It has thus generated expertise and practical know how in an industrially relevant field at the European NMIs to the sustainable benefit of the European magnetic sensor stakeholders.

Effective cooperation

The cooperation between the project partners was effective and has produced many joint presentations and publications. The different experience and instrumentation available at particular NMIs has led to joint research results which could not be achieved by an NMI alone. The metrology and particularly industrial community will profit from the joint research as it will provide more results than could be achieved by single NMIs.

Some examples for effective cooperation activities are listed below:

- Domain wall sensors were jointly investigated by PTB (fabrication), NPL (magneto transport experiments) and INRIM (micromagnetic simulations) leading to a number of publications and conference presentations.
- Micro Hall Sensors were investigated by NPL (magneto transport) and INRIM (simulations), resulting in high level publications and conference presentations.
- A new scalar 3D coil calibration method was developed in collaboration of CMI and PTB. The new procedure simple, fast and allows robust industrial on-site calibrations.
- The newly developed PTB SQUID system was used to characterise the noise figure of magnetically shielded environments developed by CMI.
- The co-operations were underpinned by mutual exchange of personnel for on-site measurements: In addition to short term visits several longer term visits of several weeks duration were carried out between INRIM, PTB, NPL and CMI: PTB scientists visited INRIM and NPL for collaborations in the field of magnetisation dynamics and SQUID measurements. INRIM scientists visited NPL and PTB for collaborations in the field of domain wall sensors and magnetisation dynamics. Furthermore a CMI researcher worked for six month at PTB in the framework of an early stage researcher mobility grant (ESRMG).

5 Website address and contact details

Project website:

http://www.ptb.de/emrp/metmags.html

Project Coordinator:

Dr. Hans Werner Schumacher

Physikalisch-Technische Bundesanstalt
Department 2.5 semiconductor Physics and Magnetism
Bundesallee 100, D-38116 Braunschweig
Germany
phone: +49-531-592-2500
fax: +49-531-592-69-2500
email: hans.w.schumacher@ptb.de

6 List of publications

- X.K. Hu, S. Sievers, A. Müller, V. Janke, and H.W. Schumacher: Classification of super domains and super domain walls in permalloy antidot lattices Physical Review B 84 024404 (2011)
- V. Panchal, K. Cedergren, R. Yakimova, A. Tzalenchuk, S. Kubatkin, and O. Kazakova: Small Epitaxial Graphene Devices for Magnetosensing Applications, Journal of Applied Physics, 2012, 111, 07E509
- A. Manzin, V. Nabaei and O. Kazakova: Modelling and optimisation of submicron Hall sensors for the detection of superparamagnetic beads, Journal of Applied Physics 2012, 111, 07E513
- A. Manzin and O. Bottauscio: Multipole expansion technique for the magnetostatic field computation in patterned magnetic films, Journal of Applied Physics 2012, 111, 07D125;
- A. Manzin and O. Bottauscio: Micromagnetic modelling of the anisotropy properties of permalloy antidot arrays with hexagonal symmetry Journal of Physics D: Applied Physics. 2012, 45, 095001;
- B. Van de Wiele, A. Manzin, A. Vansteenkiste, O. Bottauscio, L. Dupré, and D. De Zutter: A micromagnetic study of the reversal mechanism in permalloy antidot arrays, Journal of Applied Physics 2012, 111, 053915;
- N. Liebing, S. Serrano-Guisan, K. Rott, G. Reiss, J. Langer, B. Ocker, and H. W. Schumacher: Determination of spin-dependent Seebeck coefficients of CoFeB/MgO/CoFeB magnetic tunnel junction nanopillars, Journal of Applied Physics 2011, 111, 07C520 (2012),
- S. Serrano-Guisan, W. Skowronski, J. Wrona, N. Liebing, M. Czapkiewicz, T. Stobiecki, G. Reiss, and H. W. Schumacher: Inductive determination of the optimum tunnel barrier thickness in magnetic tunnelling stacks for spin torque memory applications, Journal of Applied Physics 110 2011, 110, p. 023906;
- N. Liebing, S. Serrano-Guisan, A. Caprile, E. S. Olivetti, F. Celegato, M. Pasquale, A. Müller, and H.W. Schumacher: Influence of sample geometry on inductive damping measurement methods, IEEE Transactions on Magnetics, 2011, 47, p. 2502;
- Sievers, S., Braun, K.-F., Eberbeck, D., Gustafsson, S., Olsson, E., Schumacher, H. W. and Siegner, U.: Quantitative Measurement of the Magnetic Moment of Individual Magnetic Nanoparticles by Magnetic Force Microscopy, Small,Volume 8, Issue 17, pages 2675–2679, September 10, 2012
- I. Rod, C. Wirtz, O. Kazakova, V. Panchal, D. Cox, H. Zähres, O. Posth, J. Lindner, R. Meckenstock, and M. Farle: Study of Temperature Dependence of Resistance and Noise Characteristics of a Carbon Nanotube Bolometer, Solid State Phenomena 190, 510 (2012)
- Vishal Panchal, Tim L. Burnett, Ruth Pearce, Karin Cedergren, Rositza Yakimova, Alexander Tzalenchuk, and Olga Kazakova: Surface Potential Variations in Epitaxial Graphene Devices Investigated by Electrostatic Force Spectroscopy, IEEE Transactions on Nanotechnlogy, "vol., no., pp.1,5, 20-23 Aug. 2012
- X.K. Hu, S. Sievers, A. Müller, and H.W. Schumacher: The influence of individual lattice defects on the domain structure in magnetic antidot lattices, Journal of Applied Physics, 113, 103907 (2013),
- V. Nabaei, R.K. Rajkumar, A. Manzin, O. Kazakova and A. Tzalenchuk Optimisation of Hall bar response to localized magnetic and electric fields,J. Appl. Phys Vol. 113, 064504 (2013)
- R.K. Rajkumar, A. Manzin, D.C. Cox, S.R.P Silva, A. Tzalenchuk and O. Kazakova: 3D mapping of sensitivity of graphene Hall devices to local magnetic and electrical fields, IEEE Trans. on Magn."vol.49, no.7, pp.3445,3448, July 2013
- V. Nabaei, et al.: Optimisation of Hall bar response to localized magnetic and electric fields, J. Appl. Phys "113, 064504 (2013)
- V. Panchal, et al.: Magnetic scanning probe calibration using graphene Hall sensor, IEEE Trans. on Magn. vol.49, no.7, pp.3520,3523, July 2013
- Michael Hall, Stuart Harmon and Owen Thomas, So, You Need Reliable Magnetic Measurements You Can Use With Confidence? How the Magnetic Measurement Capabilities at NPL Can Help, Journal of Magnetics (JOM), 2013, 18, (3), 339-341
- S. Sievers , N. Liebing , P.Nass , S. Serrano-Guisan , M. Pasquale , and H. W. Schumacher: Towards Wafer Scale Inductive Determination of Magnetostatic and Dynamic Parameters of Magnetic Thin Films and Multilayers, IEEE Transactions on Magnetics, Vol. 49, No. 1, January 2013
- A. Manzin and O. Bottauscio: A Micromagnetic Solver for Large-Scale Patterned Media Based on Non-Structured Meshing, IEEE Transactions on Magnetics, November 2012, Vol. 48, no. 11, pp. 2789-2792
- O. Bottauscio and A. Manzin, Spatial Reconstruction of Exchange Field Interactions With a Finite Difference Scheme Based on Unstructured Meshes, IEEE Transactions on Magnetics, November 2012, Vol. 48, no. 11, pp. 3250-3253

- L. Fricke, S. Serrano-Guisan, and H.W. Schumacher: "Parameter dependence of resonant spin torque magnetisation reversal", Physica B, condensed matter, Physica B: 407 (2012), 7, 1153 - 1156
- A. Zikmund, P.Ripka: Uncertainty analysis of calibration of the 3D coil system, Journal of Electrical Engineering, ISSN 1335 - 3632, Volume 63, 2012, p. 90-93
- V.Panchal, D.Cox, R.Yakimova,O.Kazakova: Epitaxial Graphene Sensors for Detection of Small Magnetic Moments, IEEE Trans. on Magn. Volume 49, p. 97 (2013)
- S. Bechstein, A. Kirste, D. Drung, M. Regin, O. Kazakova, J. Gallop, L. Hao, D. Cox, and T. Schurig: Investigation of Material Effects with Micro-Sized SQUID Sensors, IEEE Transactions on Applied Superconductivity Volume 23, p. 1602004 (2013).
- R.K. Rajkumar, A. Manzin, D.C. Cox, S.R.P Silva, A. Tzalenchuk and O. Kazakova: 3D mapping of sensitivity of graphene Hall devices to local magnetic and electrical fields, IEEE Trans Magn. vol. 49, no. 7, pp.3445,3448, July 2013
- N. Liebing, S. Serrano-Guisan, P. Krzysteczko, K. Rott, G. Reiss, J. Langer, B. Ocker, and H. W. Schumacher: "Tunneling magneto thermocurrent in CoFeB/MgO/CoFeB based magnetic tunnel junctions" Appl. Phys. Lett. Volume 102, p. 242413 (2013)
- A. Manzin, V. Nabaei: Modelling of micro-Hall sensors for magnetisation imaging, J. Appl. Phys. Vol. 115, 17E506, January 2014
- O. Bottauscio, A. Manzin: Parallelized micromagnetic solver for the efficient simulation of large patterned magnetic nanostructures, J. Appl. Phys. Vol. 115, 17D122, January 2014
- A. Manzin, V. Nabaei, O. Kazakova, H. Corte-León, P. Krzysteczko, H.W. Schumacher: Modeling of anisotropic magnetoresistance properties of permalloy nanostructures, IEEE Trans. Magn. Vol. 50 (4), 7100204, April 2014
- R. K. Rajkumar, A. Asenjo, V. Panchal, A. Manzin, Ó. Iglesias-Freire, O. Kazakova: Magnetic scanning gate microscopy of graphene Hall devices, J. Appl. Phys. Vol. 115, 172606 (2014)
- A. Beguivin, H. Corte-León, A. Manzin, V. Nabaei, P. Kryzstecko, H.W. Schumacher, D. Petit, R.P. Cowburn, O. Kazakova: Simultaneous magnetoresistance and magneto-optical measurements of domain wall properties in nanodevices, J. Appl. Phys. Vol. 115, 17C718, January 2014
- Christian Heiliger, Michael Czerner, Niklas Liebing, Santiago Serrano-Guisan, Karsten Rott, Günter Reiss, Hans W. Schumacher: Unusual angular dependence of tunneling magneto-Seebeck effect, arXiv:1311.2750
- X.K. Hu, P. Krzysteczko, N. Liebing, S. Serrano-Guisan, K. Rott, G. Reiss, J. Kimling, T. Böhnert, K. Nielsch, H.W. Schumacher: Magneto-thermoelectric figure of merit of Co/Cu multilayers, Applied Physics Letters, 104, 092411 (2014)
- M. Coisson, A. Manzin, G. Barrera, F. Celegato, E. Enrico, P. Tiberto, F. Vinai: Anisotropic magneto-resistance in Ni80Fe20 antidot arrays with different lattice configurations, Appl. Surf. Sci. Vol. 316, 15 October 2014, Pages 380–384
- V. Panchal, A. Lartsev, A. Manzin, R. Yakimova, A. Tzalenchuk, and O. Kazakova: Visualisation of edge effects in side-gated graphene nanodevices, Scientific Reports 4, 5881 (2014) DOI: 10.1038/srep05881
- H. Corte-León, V. Nabaei, A. Manzin, J. Fletcher, P. Krzysteczko, H. W. Schumacher, and Olga Kazakova: ‘Anisotropic Magnetoresistance State Space of Permalloy Nanowires with Domain Wall Pinning Geometry, Scientific Reports 4, Article number: 6045